Pulsating one-dimensional detonation in ammonia-hydrogen–air mixtures

Ruixuan Zhu [a], Xiaohang Fang [a,], Chao Xu [b], Majie Zhao [c], Huangwei Zhang [d], Martin Davy [a]*

[a] Department of Engineering Science, University of Oxford, Oxford, OX1 3PJ, UK
[b] Energy Systems Division, Argonne National Laboratory, Lemont, IL 60439, USA
[c] School of Aerospace Engineering, Beijing Institute of Technology, Haidian, Beijing 100081, China
[d] Department of Mechanical Engineering, National University of Singapore, 9 Engineering Drive 1, Singapore 117576, Republic of Singapore

HIGHLIGHTS

- Numerical study of one-dimensional pulsating detonation is performed.
- Ammonia and hydrogen fuel blends with various compositions are considered.
- The effects of driver pressure and fuel/air equivalence ratio are examined.
- Different pulsating detonation frequencies are observed from parametric studies.
- Chemical explosive mode analysis reveals chemistry dominates thermal diffusion at detonation front.

ARTICLE INFO

ABSTRACT

In this study, one-dimensional detonations in ammonia/hydrogen-air mixtures are numerically investigated by solving the fully compressible Navier-Stokes equations with detailed chemistry. Pulsating instabilities with single-mode are observed during the detonation wave propagation, accompanied by periodic coupling and decoupling of the lead shock wave and the reactive front. The ratio between driver pressure and initial pressure determines the overdrive degree and thus the oscillatory mode of detonation for a premixture with certain composition. The effects of hydrogen dilution and mixture equivalence ratio on pulsating detonations are also examined under a constant driver pressure. The growing hydrogen fraction in fuel blends significantly increases the oscillation frequency. In addition, the pulsating detonation frequency rises with increasing equivalence ratio under fuel-lean conditions, peaks under stoichiometric conditions, and falls under fuel-rich conditions as the equivalence ratio increases further. Evolutions of reactants, main intermediate radicals, and products are analysed in both fuel-lean and fuel-rich conditions. A chemical explosive mode analysis further confirms the highly-autoignitive nature of the mixture in the induction zone between reaction front and shock front where thermal diffusion plays a negligible role.

Please cite this article as: Zhu R et al., Pulsating one-dimensional detonation in ammonia-hydrogen–air mixtures, International Journal of Hydrogen Energy, https://doi.org/10.1016/j.ijhydene.2022.04.265

Introduction

Detonation engines, e.g. pulse detonation engines (PDE) [1] and rotating detonation engines (RDE) [2], have received significant research interest for several decades. The utilisation of detonation for air-breathing propulsion would require steady forward propagating detonation waves. The basic structure of a stable detonation wave can be described using the Zeldovich−von Neumann−Döring (ZND) model, which consists of a leading shock and a trailing reaction zone. In this model, the minimum sustainable detonation speed is known as the Chapman-Jouguet (CJ) speed [3]. However, while the ZND model assumes a stable detonation wave, both experimental and numerical studies have shown that real detonation waves are unstable with flow perturbations [4]. Temporal and spatial instabilities in complex detonation systems, including three-dimensional (3D) cellular structures and one-dimensional (1D) pulsating (galloping) detonations, are found in practical systems. Pulsating instability with longitudinal oscillations of the detonation front has also been experimentally observed when a blunt body travels through a reactive gas at near CJ velocities [5,6]. While prior studies have suggested that a detonation is three-dimensional in nature, transient, multi-dimensional numerical simulations with adequate mesh resolution that solve the exothermic reaction layer and the complex wave structures are still challenging. Previous studies have suggested that 1D pulsating detonation with periodic longitudinal variations of the coupled shock wave and reaction zone should be associated with 3D cellular structures [7]. Thus, fully resolved simulations of 1D detonation, which is representative of the complicated physics involved in unstable detonation propagation, can further the understanding of detonation initiation and wave interactions in pulsating detonations.

The sensitivity analysis of steady planar detonations to perturbations was pioneered by Erpenbeck via linear stability theory based on 1D simulations with an idealised single irreversible reaction, and Arrhenius reaction rate [8]. Since then, different oscillatory modes have been studied in 1D piston-supported overdriven pulsating detonations [9]. McVey and Toong [10] and Alpert and Toong [11] developed a two-zone detonation structure theory, which indicates that the lead shock and the intense chemical reaction zone are separated by a thermally neutral induction zone. The McVey-Toong wave-interaction theory suggested that the detonative pulsating instability is caused by the periodic wave interactions behind the lead shock. Bourlioux et al. [12] later highlighted that pulsating detonations tend to occur at lower degrees of overdrive while steady solutions are more likely to be achieved through highly overdriven detonation waves. The numerical studies of He and Lee [13] further showed that a detonation wave fails to be self-sustained with an autoignition mechanism when overdrive degrees are too low. At these failed regimes, the oscillatory period becomes infinitely large.

The above numerical studies mainly focused on oscillation modes via the shock pressure development calculated with the simplified one-step chemistry. With one-step chemistry, a distributed heat release occurs in the detonation reaction zone, where the detonation structure is controlled by the activation energy only. However, practical gaseous detonation involves chain-branching reactions, primarily in an induction zone, where radical species proliferate, followed by a reaction zone, where radicals recombine and release a large amount of energy. Sanchez et al. [14] applied a three-step chain-branching reaction model to pulsating detonations and found that the ratio of chain-branching induction length to the length of the exothermic recombination zone determines the stability and oscillatory mode. Ng et al. [15] observed similar phenomena via two-step chemistry where unstable detonations tend to occur when the induction zone dominates the reaction zone. They further defined a stability parameter as the activation energy for the induction process multiplied by the ratio of the induction length to the reaction length. Leung et al. [16] also highlighted a novel regime with a pulsation period smaller than the induction time using a two-step chain-branching model with separate induction and reaction zones. These studies indicate that the complex interactions between chemical kinetics and wave structures play important roles in unstable detonations. The utilisation of realistic chemistry can therefore help improve the understanding of initiation, branching, and recombination characteristics at the shock-flame front.

A series of numerical studies with more detailed chemical reaction models have further elucidated pulsating detonation mechanisms. Sussman [17] observed two oscillation modes in stoichiometric hydrogen-air mixtures that depend on the ratio of the heat release time to the induction time with detailed chemistry. Yungster and Radhakrishnan [18] studied the high-frequency and small-amplitude pulsating mode in hydrogen-air mixtures where small unreacted pockets behind the over-driven front were observed. By applying the Euler and the diffusive Navier-Stokes (NS) equations with a detailed hydrogen-oxygen mechanism, Han et al. [19] pointed out that diffusion can have a relatively prominent role in the burning of unreacted hydrogen pockets. Romick et al. [20] also verified the major role that the physical mass, momentum, and energy diffusion play in highly unstable 1D piston-driven hydrogen-air detonations due to unburned hydrogen pockets. Many studies with more detailed chemistry have proved the significant effects of premixture compositions, overdrive degrees, and initial conditions on oscillatory modes of unstable detonation propagation in hydrogen blends [18,21]. More recently, Ma et al. [22] found that the mixture inhomogeneity has significant effects on the pulsating behaviour due to the interaction of the leading shock and the local gradient in a hydrogen-oxygen mixture with a sinusoidal distribution of hydrogen molar fraction. Pulsating detonations in realistic hydrocarbon fuels have also been investigated with detailed chemistry models containing many chemical reactions and intermediates. Radulescu et al. [23] numerically studied 1D acetylene-oxygen pulsating detonations and found that the detonations become unstable as the argon dilution decreases. Zhao et al. [24] observed the low-frequency oscillatory mode in both fuel-lean and fuel-rich *n*-heptane/air mixtures, but the stable detonation propagation mode for near-stoichiometric conditions.

Hydrogen, as a promising clean fuel for detonation propulsion engines, has attracted most research efforts over the years as mentioned above due to its high chemical reactivity, wide flammability limit and low ignition energy [25]. Experiments and Numerical studies have found the addition of hydrogen can enhance the ignition and combustion

performances of some hydrocarbon fuels, such as methane [26,27], propane [28]. and various liquid fuels [29]. However, the shortfalls associated with hydrogen storage and supply have driven researchers to explore other sustainable fuel sources. Ammonia has been recognised as a hydrogen carrier with a high potential for development. The study of ammonia as a fuel for propulsion systems can be dated back to the middle of 20th century. Liquid ammonia was found to be a stable fuel with good volumetric energy density, cooling properties, and potential for hydrogen engine development. Rocket fuel studies with a combination of acetylene and liquid ammonia also showed a great improvement in fuel properties and, more importantly, higher stability when compared to other fuel blends at various conditions during launch. Recently, there has been renewed interest in the development of ammonia, as a carbon-free fuel, for combustion systems [30,31] where hydrogen/nitrogen/ammonia/air mixtures have been shown to have similar combustion characteristics as gasoline [32]. Recent numerical studies have also observed end-gas autoignition and deflagration-to-detonation transition phenomena in ammonia-hydrogen-oxygen/air mixtures [33,34] where the explosion pressure of hydrogen/ammonia fuel is evaluated by Li et al. [35]. While nitrogen oxides (NO$_x$) emissions are one of the major concerns when using ammonia as a fuel, studies have found that NO$_x$ emissions from ammonia-hydrogen blends can considerably decrease from medium pressure to high pressure, while slightly rising with increasing temperature [36]. As the pressure and temperature of detonative combustion is much higher than those of deflagration, it is attractive to study the possibility of using ammonia-hydrogen blends in detonation-based engines.

Literature on using ammonia as a propulsion fuel is still scarce as the feasibility and safety of its application in detonation propulsion systems are still not well understood. Therefore, the objective of this work is to understand the complex physics and shock-flame interactions in pulsating detonations for ammonia-hydrogen-air mixtures via 1D simulations and the chemical explosive mode analysis (CEMA). This study is the first step to understand the feasibility of using ammonia-hydrogen blends as the fuel for detonation-based engines. Navier-Stokes equations with detailed chemistry solver for ammonia and hydrogen oxidation will be solved. The influence of premixture compositions, including the volume fraction of hydrogen in fuel and equivalence ratio, on pulsating detonation, will be investigated. The rest of this paper is organised as follows: the governing equations, numerical method, and computational setup are introduced in Section Modelling details, followed by the presentation and discussion of simulation results in Section Results and discussion. Conclusions are drawn in Section Conclusions.

Modelling details

Governing equations

Fully compressible Navier-Stokes equations of mass, momentum, energy, and species mass fraction are solved for multi-component, reacting flows, read as:

$$\frac{\partial \rho}{\partial t} + \nabla \cdot (\rho \mathbf{u}) = 0 \tag{1}$$

$$\frac{\partial (\rho \mathbf{u})}{\partial t} + \nabla \cdot (\mathbf{u}(\rho \mathbf{u})) + \nabla p - \nabla \cdot \tau = 0 \tag{2}$$

$$\frac{\partial (\rho E)}{\partial t} + \nabla \cdot (\mathbf{u}(\rho E)) + \nabla \cdot (\mathbf{u}p) - \nabla \cdot (\tau \cdot \mathbf{u}) - \nabla \cdot (k \nabla T) = \dot{\omega}_T \tag{3}$$

$$\frac{\partial (\rho Y_i)}{\partial t} + \nabla \cdot (\mathbf{u}(\rho Y_i)) - \nabla \cdot (\rho D \nabla Y_i) = \dot{\omega}_i, (i = 1, \cdots N) \tag{4}$$

$$p = \frac{\rho R T}{M} \tag{5}$$

Where t, ρ, $\mathbf{u}$, p, T and E refer to the time, density, velocity vector, gas pressure, temperature, and total non-chemical energy, respectively. R and M in Eq. (5) refer to the universal gas constant and the molar weight of the mixture, respectively. The viscous tensor, τ, in Eq. (2) is modelled as

$$\tau = \mu \left(\nabla \mathbf{u} + (\nabla \mathbf{u})^T - \frac{2}{3} (\nabla \cdot \mathbf{u}) \mathbf{I} \right) \tag{6}$$

Here the dynamic viscosity μ is estimated via Sutherland's law, $\mu = A_s \sqrt{T}/(1 + T_s/T)$, where $A_s = 1.67212 \times 10^{-6}$ kg/m·s·$\sqrt{K}$ and $T_s = 170.672$ K are respectively the Sutherland coefficient and the Sutherland temperature. The thermal conductivity, k, in Eq. (3) is estimated based on the Eucken approximation [37] as

$$k = \mu C_v (1.32 + 1.37 R / C_v) \tag{7}$$

With unity Lewis number assumption, the mass diffusion, D, in Eq. (4) is calculated by

$$D = \alpha = k / \rho C_p \tag{8}$$

Here C_v and C_p refer to the heat capacity at constant volume, and at constant pressure, respectively. $\dot{\omega}_T$ in Eq. (3) accounts for the combustion heat release and the net production rate of i-th species in Eq. (4) is given by $\dot{\omega}_i$.

Numerical methods

The governing equations, i.e. Eqs. (1)–(4) are solved with a density-based, multi-component reactive solver, *RYrhoCentralFoam* [38], which was developed based on the standard compressible flow solver, *rhoCentralFoam* [39], in the open-source CFD toolbox OpenFOAM 6.0. The finite volume method is used for the spatial discretisation. The numerical flux of the convective term is calculated using a second-order, non-staggered, Godunov-type central-upwind scheme, known as the Kurganov, Noelle, and Petrova [40] (KNP) method. A Van Leer limiter is adopted for correcting flux calculations by the KNP method. Detailed chemistry calculations are performed, and the convective terms in the energy and species mass fraction equations are solved with a total variation diminishing scheme to ensure the scalar boundness. The diffusive terms in Eqs. (1)–(4) are calculated with a second-order central differencing scheme. The chemical source terms are obtained by integrating local chemical

ordinary differential equations with a stiff solver, i.e. Seulex solver [41]. A semi-implicit second-order scheme is applied for time discretisation. The maximum Courant number is adjusted between 0.02 and 0.05 according to mesh resolutions, which results in the maximum physical time step of approximately 10^{-9} s.

The original non-reacting solver, *rhoCentralFoam*, has been validated by Greenshields et al. [39] in 1D shock tube and 2D forward-facing step simulations. The reactive solver, *RYrhoCentralFoam* [38,42], was proved to be able to accurately predict the statistics of the velocity and/or reactive scalar fields of laboratory-scale supersonic hydrogen-air autoigniting flames [43] and a model supersonic combustor [44]. Moreover, the capability of the solver to capture flow discontinuities (e.g. shock wave and expansion wave), autoignition, and shock-induced ignition, has also been demonstrated via rotating detonation simulations by capturing the transient behaviours of detonation wave propagation [45,46]. The solver has been recently adopted in the study of pulsating propagation and extinction of hydrogen detonations in water sprays by Xu et al. [47,48]. This solver also accurately predicted various oscillatory modes for 1D pulsating detonation in *n*-heptane-air mixtures under off-stoichiometric conditions [24]. For this study, the reactive solver is coupled with a detailed chemical mechanism for ammonia-hydrogen blends. The mechanism, with 34 species and 204 elementary reactions, was developed by Song et al. [49] and has previously been applied to studies of ammonia-hydrogen oxidation at high pressure and temperature conditions in a jet stirred flow reactor [50,51].

Computational setup

Pulsating detonation propagation in ammonia-hydrogen-air mixtures under different conditions is numerically studied in a one-dimensional detonation tube. Fig. 1 shows the schematic of the computational domain. The detonation tube is closed at the left end and the right end. In this study a high-pressure (p_{drive}), high-temperature (2500 K) hot spot (2 mm thick) is placed at the left end of the detonation tube to initiate the detonation wave. The hot spot is chosen to initiate a right-propagating detonation in the domain. The validity of this ignition method was previously studied by Yungster and Radhakrishnan [18,52] for hydrogen-air and ethylene-air mixtures. The initial velocity is set to be zero, and the ammonia-hydrogen-air mixture ahead of the detonation wave is in a quiescent state. Zero-gradient conditions are enforced for all variables at both the left and right boundaries of the domain.

The initial composition of premixtures is parameterised through the volume fraction of hydrogen in ammonia-hydrogen blends (X_{H_2}) and the equivalence ratio (ϕ). The dilution effect of hydrogen is studied by varying the hydrogen volume fraction from 0.2 to 0.7. The effects of mixture strength on pulsating detonations are studied by varying the equivalence ratio from 0.6 to 2.5. The initial temperature of the unburned mixture is 300 K, and the initial pressure is 1 atm. The length of the detonation tube (L) shown in Fig. 1 is adjusted with respect to the mixture composition to ensure sufficiently long detonation propagation and long-lasting pulsation phenomenon due to the varying unsteady characteristics (e.g., pulsating period). For example, L is 1.5 m for $\phi = 0.8$, but longer for leaner mixtures (2.5 m for $\phi = 0.6$) with $X_{H_2} = 0.2$.

Results and discussion

Grid convergence tests

In order to fully resolve detonation structures and wave interactions in the induction zone, an adequate mesh resolution for each case is needed. Therefore, the effects of spatial resolution on ammonia-hydrogen blend pulsating detonations are first studied. A baseline case when $X_{H_2} = 0.2$, $\phi = 0.8$ is selected for the analysis of mesh resolution. The grid size needed for each condition is estimated via the Half-Reaction Length (HRL) of the ZND structure, defined as the distance from the leading shock front to the location of peak heat release rate. Previous studies of 1D ZND detonation for ammonia suggested the HRL can vary considerably with the initial composition of mixtures [53]. Therefore, ZND structures
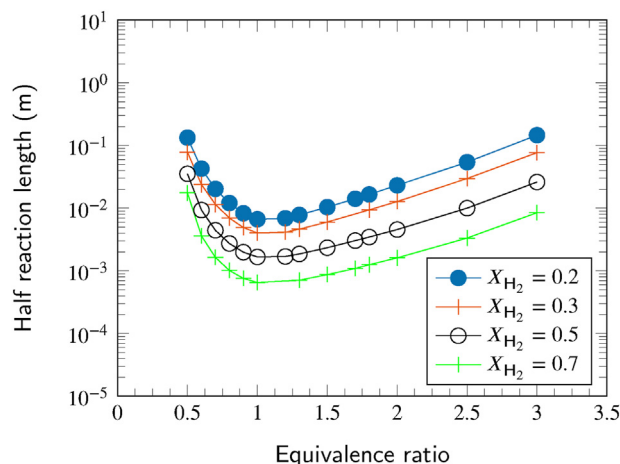
Fig. 2 − **Half-reaction length as a function of fuel/air equivalence ratio and volume fraction of hydrogen in fuel (initial temperature: 300 K, initial pressure: 1 atm).**
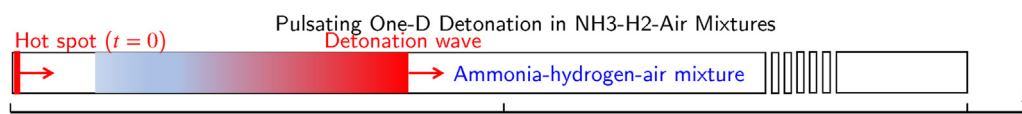
Fig. 1 − **Schematic of one-dimensional detonation tube. The red pocket with high temperature (2500 K) and high pressure (p_{drive}) is the hot spot to initiate the flame. The initial gas is ammonia-hydrogen-air premixtures. (For interpretation of the references to colour in this figure legend, the reader is referred to the Web version of this article.)**

of 1D detonations for different mixtures are first calculated via the Shock and Detonation Toolbox [54]. Significant variation of HRL ($L_{1/2}$) as a function of fuel/air equivalence ratio and volume fraction of hydrogen in fuel can be observed in Fig. 2. For a fixed hydrogen mass fraction and initial pressure, HRL reaches a minimum around stoichiometry while larger HRL is found for lean and rich conditions. Increasing hydrogen mass fraction also lowers the value of HRL. This indicates that the reactivity of the mixture rises when the X_{H_2} is increased, resulting in shorter ignition delay and induction length.

Grid convergence tests are performed on the 1D pulsating detonation for $X_{H_2} = 0.2$, $\phi = 0.8$, $p_0 = 1$ atm and $T_0 = 300$ K. The driver pressure at the hot spot is first set to 150 atm. Four different meshes with uniform cell sizes of 0.3 mm, 0.15 mm, 0.08 mm, and 0.04 mm are selected, corresponding to 40, 80, 150, and 300 computational grids per HRL (12.04 mm for this condition). Fig. 3 shows the time histories of pressure at the leading shock front (referred to as the shock pressure) with different mesh sizes. The position of leading shock is identified where the pressure gradient is maximum. As shown in Fig. 3, stable detonation with slight pressure variations is observed at 40 cells/$L_{1/2}$, whereas, pulsating detonations with constant oscillatory frequencies are captured with all other three mesh resolutions. Similar pulsating frequencies exist for 150 cells/$L_{1/2}$ and 300 cells/$L_{1/2}$, though lower peak values of shock pressure are predicted with 150 cells/$L_{1/2}$. The oscillatory frequency is slightly under-predicted for 80 cells/$L_{1/2}$, and a further reduction in peak shock pressure is observed. Therefore, a mesh resolution between 150 cells/$L_{1/2}$ and 300 cells/$L_{1/2}$ is adopted for all following studies balancing numerical accuracy and computational cost.

Effects of hydrogen volume fraction in fuel

In this study, the effect of hydrogen addition in ammonia for pulsating detonation is investigated. The ratio between the high driver pressure (p_{drive}) and the initial pressure in the
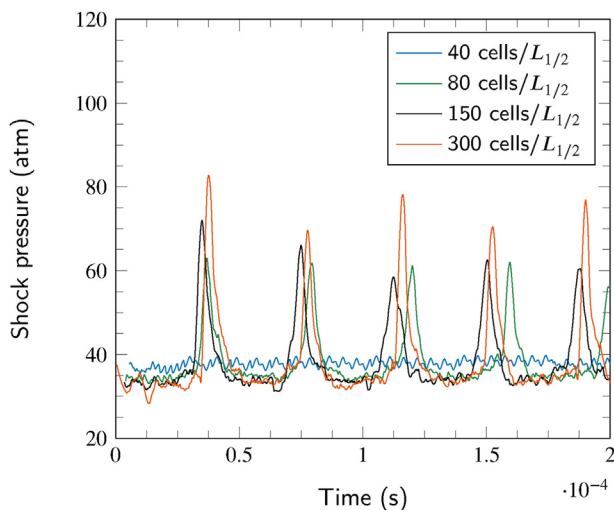
Fig. 3 — Time history of shock pressure with different mesh sizes (initial temperature: 300 K, initial pressure: 1 atm, volume fraction of hydrogen in fuel: 0.2, equivalence ratio: 0.8).
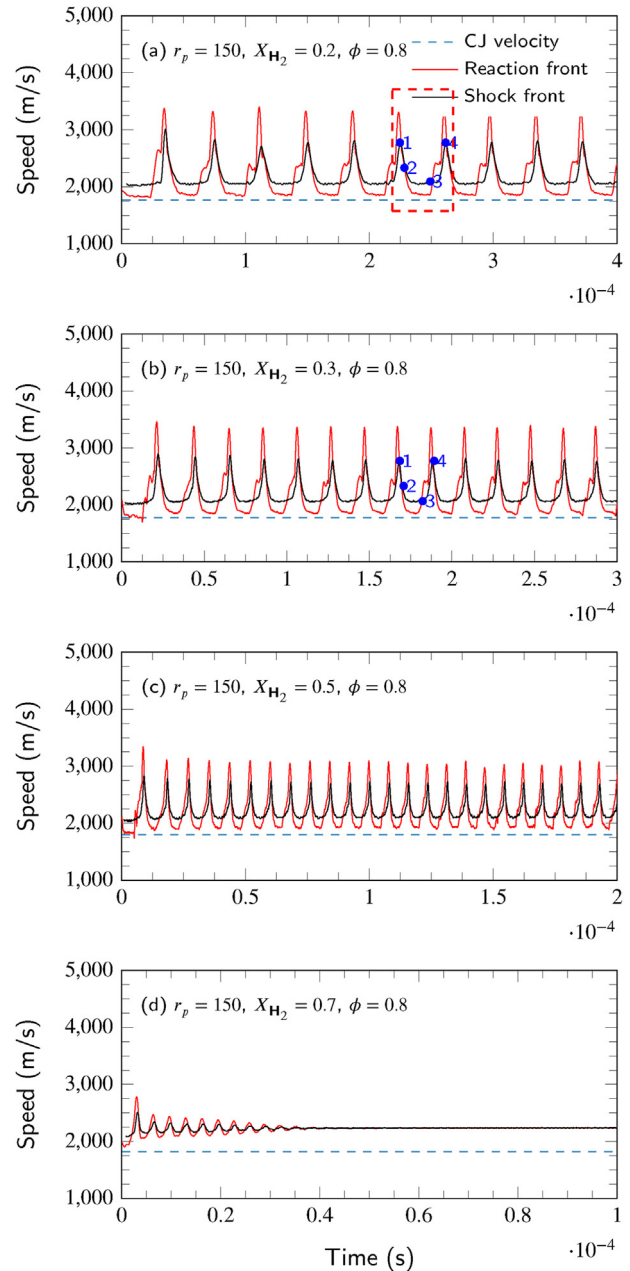
Fig. 4 — Time histories of propagation speeds of reaction and shock fronts with volume fraction of hydrogen in fuel of (a) $X_{H_2} = 0.2$, (b) $X_{H_2} = 0.3$, (c) $X_{H_2} = 0.5$, (d) $X_{H_2} = 0.7$ (initial temperature: 300 K, initial pressure: 1 atm, equivalence ratio: 0.8).

detonation tube ($r_p = p_{\text{drive}}/p_0$) is set to be 150 for all the simulations, and the effect of the driver pressure can be found in Appendix. Fig. 4 shows the temporal evolution of the reaction front (RF) and shock front (SF) pulsating propagation speeds of various hydrogen volume fractions, i.e. $X_{H_2} = 0.2 - 0.7$, in ammonia-hydrogen blends (initial conditions at: p_0, r_p, T_0, $\phi = 1$ atm, 150, 300 K, 0.8). Here, the position of the RF is defined as that of the maximum heat release rate (HRR) in the detonation tube. Significant pulsating instabilities of RF and SF propagation are observed for relatively low volume fractions of hydrogen in fuel when $X_{H_2} = 0.2, 0.3$ and 0.5. For the

same driver pressure ratio of 150, stable detonation with a constant propagation speed can be achieved when X_{H_2} is increased to 0.7. While the results shown here suggest the detonation stability would monotonically increase with the increasing volume fraction of hydrogen, previous studies have pointed out that for pure hydrogen-air mixtures detonation did not reach stability until a higher drive ratio of 200 [18]. This indicates addition of ammonia in hydrogen-air mixture can possibly stabilise detonation waves at a lower drive ratio. However, the optimal mixture ratio for each condition to reach stability would require further investigations. The CJ speed (D_{CJ}), overdrive degree (f), oscillation frequency (ω) and amplitude ($\Delta p/p$) for all conditions tested in this study are summarised in Table 1. The overdrive degree is defined as $f = D^2/D_{CJ}^2$, where D is the actual detonation propagation speed and D_{CJ} refers to the theoretical Chapman-Jouguet detonation speed. The oscillatory amplitude is given by $\Delta p/p$, where Δp is the computed peak-to-trough shock pressure and p is the computed average value. A slight increase in CJ speed is observed for the increasing hydrogen volume fraction together with increasing average propagation speeds of RF and SF. The oscillation frequency dramatically rises with a growing hydrogen fraction. The overdrive degree of SF is found to minimally affected by the X_{H_2} in fuel-lean ammonia-hydrogen-air mixtures ($\phi = 0.8$). The $\Delta p/p$ of SF only decreases from 0.77 for $X_{H_2} = 0.2$ to 0.69 for $X_{H_2} = 0.5$ with small fluctuations.

To further study the effect of hydrogen addition, the interactions between RF and SF are detailed for different hydrogen volume fractions, as shown in Fig. 4. The coupling of RF and SF can be roughly characterised by equal speeds of the two fronts (i.e. intersections labelled 1, 2, 3, 4) as indicated in Fig. 4(a) and (b). The RF always accelerates slightly earlier than the SF within each pulsating detonation cycle. The period between instants 1 and 2 corresponds to detonative combustion when the two coupled fronts synchronously propagate forward (coupling period). Between instants 2 and 4, RF and SF are decoupled, featured by their distinct speeds (decoupling period). The RF speed catches up with SF speed at instant 3. According to this, the decoupling period can be further divided into two stages: accelerated decoupling (i.e. 2-3) and accelerated recoupling (i.e. 3-4) periods. Accelerated decoupling is characterised by gradually increasing distance between the RF and SF as the trailing RF travels slower than the lead SF, while accelerated recoupling corresponds to the gradual approaching of the two travelling fronts. The coupling interval (T_c) and decoupling interval (T_d) last about 0.002 ms (0.167−0.169 ms)

and 0.019 ms (0.169−0.188 ms) for $X_{H_2} = 0.3$ and $\phi = 0.8$, respectively. The coupling period accounts for about 10% of the whole pulsating detonation cycle for $X_{H_2} = 0.3$ compared to 14% ($T_c = 0.005$ ms, $T_d = 0.032$ ms) for $X_{H_2} = 0.2$, suggesting the pulsating detonation cycle is shortened with increasing X_{H_2} accompanied by reduced the proportion of T_c. Previous studies highlighted that the decrease in activation energy could shorten the intervals between the death and re-initiation of pulsating detonation [13], suggesting the addition of hydrogen in ammonia reduces the activation energy of the blends for pulsating detonation.

Fig. 5 depicts the spatial and temporal distributions of temperature, pressure gradient, density gradient, and hydroxide (OH) mass fraction in one pulsating detonation cycle marked by the dashed boxed area in Fig. 4(a). The reactive front and the lead shock wave demonstrate a coupling duration (T_c) and a relatively long decoupling duration (T_d), as seen in Fig. 5(a). The coupling or decoupling instants, similar to the criteria set out in the literature [24,55], are identified based on the distance between the RF and the SF; in this case, distances less than 0.1 mm are considered as coupled, otherwise considered as decoupled. The T_d lasts about 0.032 ms, which is much longer than T_c of 0.005 ms. It is also observed from 5(a) that the temperature of the RF is significantly elevated when SF is coupled with RF within the short T_c duration, while reduced when the two fronts are decoupled. A larger amount of OH is also produced near the high-temperature RF within the T_c period than that of the T_d period, as seen in Fig. 5(d). Moreover, the secondary reaction front (SRF) in Fig. 5(a) and (d) can be clearly observed with changes of temperature and OH concentration across it. The SRF stems from the continuous chemical reactions of undetonated intermediate radicals behind the RF, and the temperature behind it can reach 3000 K.

The dynamic behaviour and complex interactions of the RF and SF within the pulsating cycle can be presented via pressure and density gradients shown in Fig. 5(b) and (c). The early part of T_d is the accelerated decoupling stage, and the rest is the accelerated recoupling stage, separated by the first bifurcation (labelled as B_1) in Fig. 5(b). B_1 occurs at around 0.250 ms when a new SF forms ahead of the RF, which is a developing detonative front accompanied by the formation of a series of compression waves (i.e. CW_1). The new detonative front moves faster than and gets closer to the old SF between B_1 and the second bifurcation (i.e. B_2) at around 0.260 ms. The heat release rate (HRR) between them increases due to compression effects until the old SF turns into another detonative front together with a new RF in the shocked gas at B_2, accompanied by the formation of the second series of compression waves (i.e. CW_2). In the meantime, the first new-formed developing detonative front degenerates into an intense reaction front with high HRR as the pressure growth across it is not sufficient enough to support a detonation wave. These compression waves, CW_1 and CW_2 (termed as "reaction shock" by Alpert and Toong [6]), are caused by rapid heat release around detonative fronts. This phenomenon of a detonative front leading an intense RF is marked with a circle in Fig. 5(c), and will be further presented in Fig. 6. The third bifurcation B_3 occurs at around 0.262 ms when the trailing reaction front merges into the lead detonative front and produces the

Table 1 − The CJ speed, overdrive degree, oscillation frequency and amplitude for various hydrogen volume fraction in fuel ($\phi = 0.8$, $p_0 = 1$ atm, $r_p = 150$, $T_0 = 300$ K).

| X_{H_2}	D_{CJ} (m/s)	f	ω (Hz)	$\Delta p/p$
0.2	1767.21	1.53	27027	0.77
0.3	1776.44	1.54	52632	0.79
0.5	1796.83	1.55	126582	0.69
0.7	1820.21	1.51	N.A.	N.A.
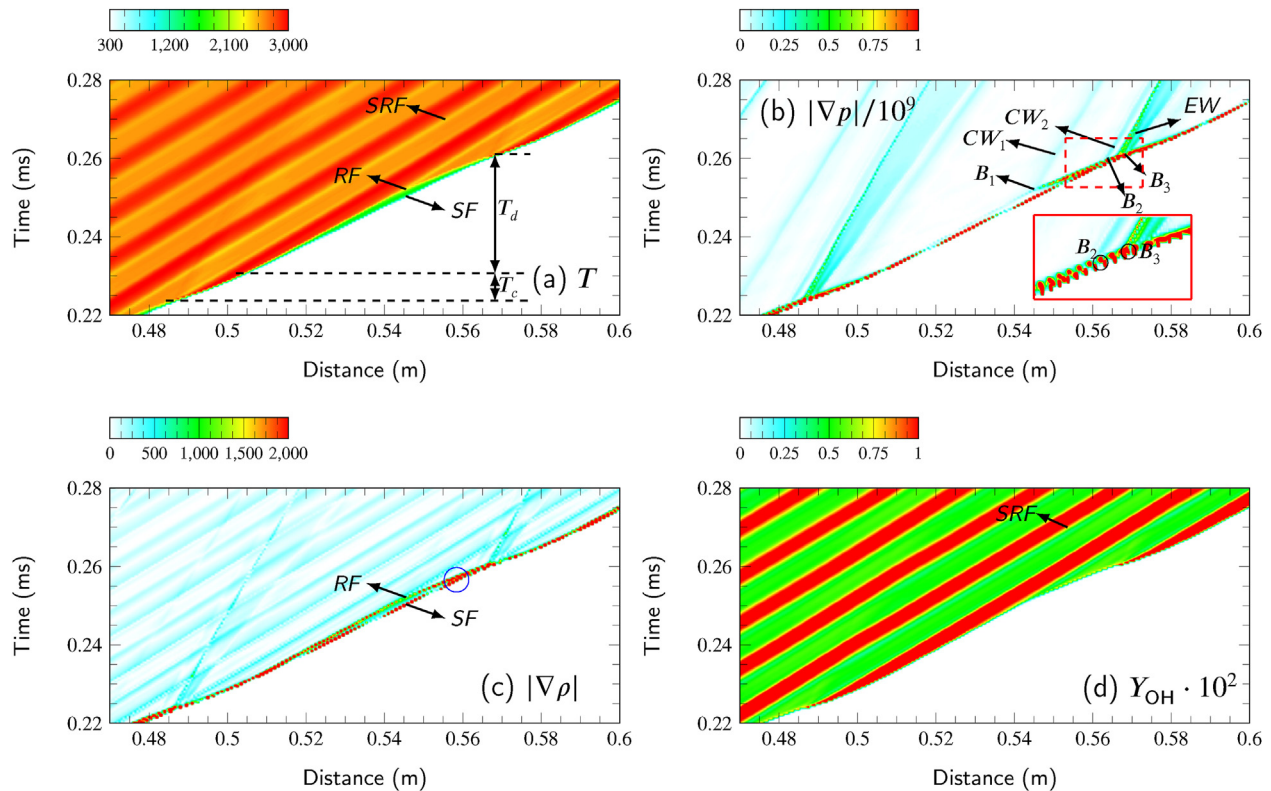
Fig. 5 – Spatial and temporal distributions of (a) temperature (in K), (b) pressure gradient (Pa/m), (c) density gradient (kg/m⁴), (d) mass fraction of OH. RF: reaction front; SRF: secondary reaction front; SF: shock front; CW_1, CW_2: compression waves; EW: expansion wave; T_D: decoupling period; T_C: coupling period; B_1, B_2, B_3: bifurcation point (hydrogen volume fraction: 0.2, equivalence ratio: 0.8, initial temperature: 300 K, initial pressure: 1 atm).

detonation wave for the next pulsating detonation cycle, and it generates a backward-propagating expansion wave (EW) relative to the lead SF. The complex interactions of EW, CW_1, and CW_2 are generated periodically within each pulsation cycle, which leads to spatial pressure fluctuations behind the detonation wave. The foregoing process of new detonation wave formation roughly happens in each accelerated recoupling period.

The spatial distributions of pressure and temperature around B_2 (0.26 ms) and B_3 (0.262 ms) with HRR curves are shown in Fig. 6. The left-propagating compression waves (e.g. CW_1 and CW_2) relative to the RF are observed, and the intensity of CW_2 is much higher than that of CW_1. The two peak values of HRR at the RF (i.e. at 0.566 m) of detonative front ahead and the following intense reaction front (i.e. 0.565 m) are almost the same in Fig. 6(a) at 0.260 ms, which corresponds to the phenomenon observed in Fig. 5(b) and (c). The temperature between two peaks of HRR slightly decreases first as it crosses the lead forward-propagating detonative front; then a pronounced temperature rise is observed, arising from the intense reaction front with strong heat release as shown in Fig. 6(b). This reaction front wave later combines with the lead detonative front and they evolve into a new detonation wave at 0.262 ms for the next pulsating detonation cycle, together with the generation of the expansion wave EW in Fig. 6(c). In addition, the intensity of CW_2 decreases from 0.26 ms to 0.262 ms as it moves backward relative to the SF.

To further elaborate the unsteady physics in one pulsating detonation cycle for different ammonia-hydrogen blends, Fig. 7(a)-(c) and (d)-(e) show periodic spatial variations of the pressure, temperature and HRR under $X_{H_2} = 0.2$ and $X_{H_2} = 0.5$, respectively. The shock pressure in Fig. 7(a) first decreases from 0.225 ms (line #1) to 0.230 ms (line #3) within the coupling period (T_c), accompanied with evident HRR decrease in Fig. 7(c). During the accelerated decoupling period between 0.230 ms (line #3) and 0.250 ms (line #7), the shock pressure levels off, and the HRR of the RF is continuously reduced. At these instants, the locations of peak HRR slightly lag behind those of the leading SF where the pressure jumps, which travels faster than the RF marked by the red dashed line in Fig. 7(a)−(c). Meanwhile, a two-stage growth of the temperature profile is observed in Fig. 7(b), induced by the SF compression effects and the heat release of trailing RF, respectively. The accelerated recoupling period happens from 0.250 ms (line #7) to 0.262 ms (line #11). After B_1 in Fig. 5(b) at 0.250 ms, localised pressure rise is observed just ahead of the peak HRR of RF (marked with the black dashed line) at 0.255 ms (line #8), resulting in a new detonative front, and thus the previous SF turns into a lead shock wave. A new RF with increasing HRR occurs closely downstream of the lead shock wave at 0.259 ms (line #9) and later produces another new detonative front at 0.260 ms (line #10) when it almost has the same peak HRR of 1.5×10^{13} J/m³/s as the RF of the following detonative front, which accords with B_2 in Fig. 5(b). At the
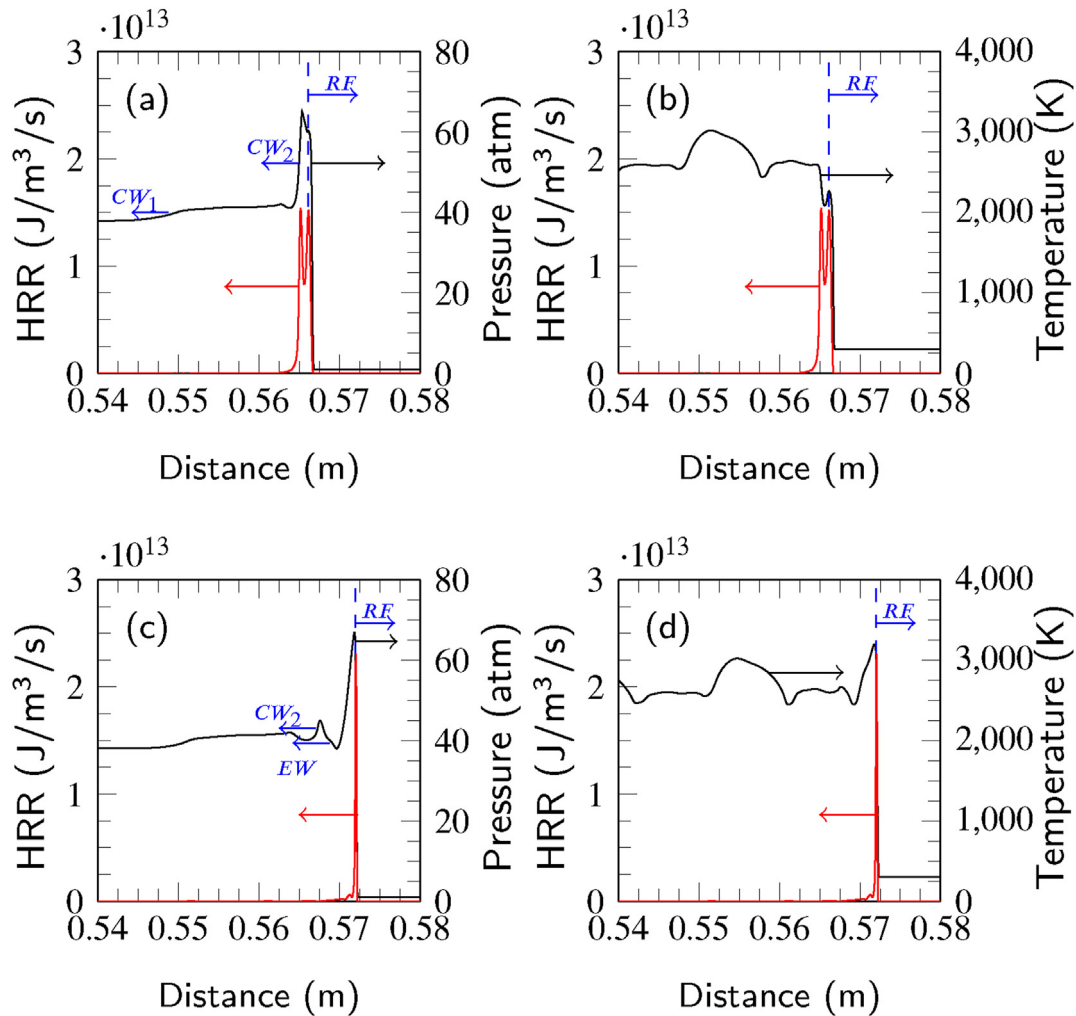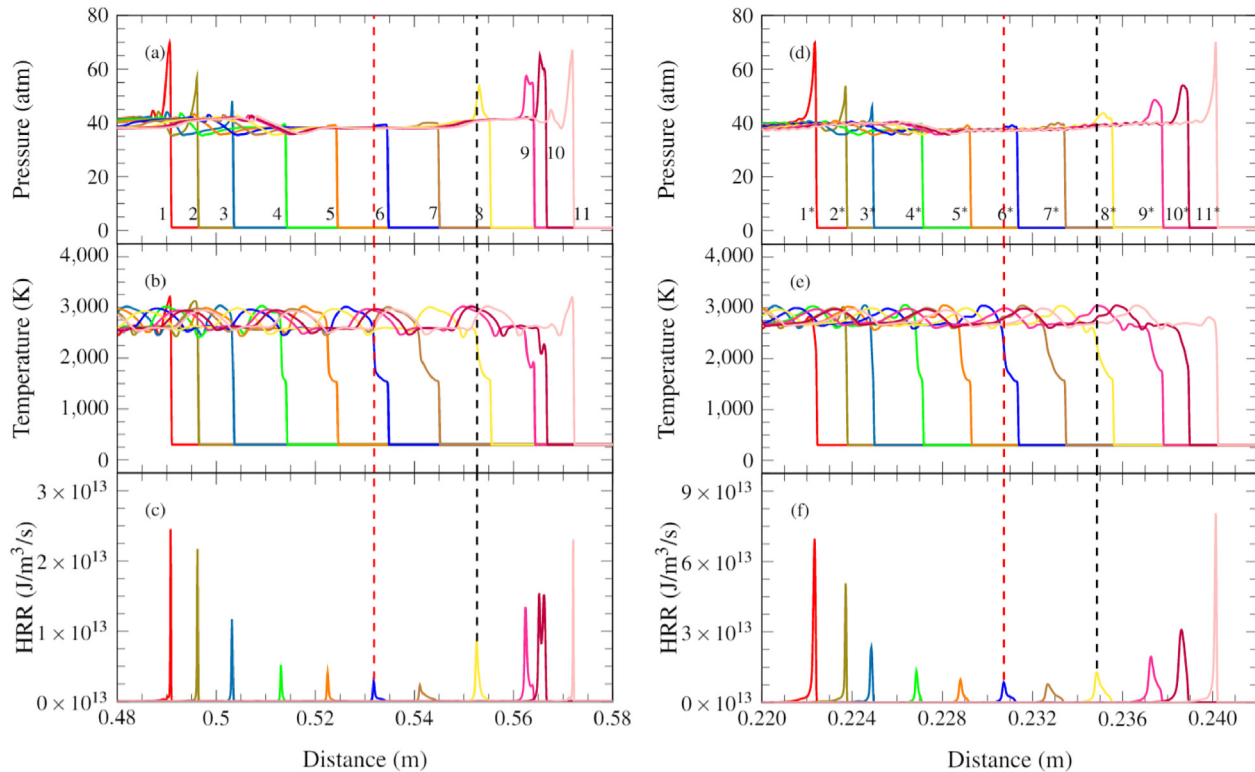
Fig. 6 − Spatial profiles of heat release rate and (a) pressure, (b) temperature at t = 0.260 ms, and (c) pressure, (d) temperature at t = 0.262 ms (hydrogen volume fraction: 0.2, equivalence ratio: 0.8, initial temperature: 300 K, initial pressure: 1 atm).

same time, the previously newly-formed detonative wave decays into an intense reaction front with high HRR, which finally penetrates into the later-formed lead detonative front at 0.262 ms, concurrently B_3 is generated, as shown in Fig. 5(b). The shock pressure, shock temperature and HRR get back to 66.88 atm, 3100 K and 2.3 × 10^{13} J/m^3/s, respectively, as the detonation wave of coupled RF and SF is reinitiated, and then the next repeated process starts. In addition, the spatial fluctuations of temperature behind the detonation wave at 0.225 or 0.265 ms within T_c are in line with those of pressure, caused by the complex of EW, CW_1, and CW_2 generated in each pulsation cycle. Such phenomena were also observed by Sharpe and Falle [56] by 1D pathological detonation simulation and termed as "explosions in the explosion", which is related to the pockets of partly burned fuels in the shocked gas when the activation temperature is high or a constant energy addition is supported by the piston.

Likewise, the spatial distributions of pressure, temperature and HRR in a pulsating detonation cycle for $X_{H_2} = 0.5$ are successively presented in Fig. 7(d)−(f). Similar unsteady phenomena to those for $X_{H_2} = 0.2$ are observed in the coupling (i.e. line #1*-3* from 0.1 ms to 0.101 ms) and accelerated decoupling durations (i.e. line #3*-7* from 0.101 ms to 0.105 ms). The values of both the SF pressure and RF temperature of detonation for $X_{H_2} = 0.5$ are close to those for $X_{H_2} = 0.2$ during T_c, at around 70 atm and 2825 K; however, the HRR is much higher here (6.97 × 10^{13} J/m^3/s), stemming from the high chemical energy pulse from hydrogen addition. A significant pressure increase, i.e. the SF, is observed ahead of the RF at 0.104 ms (line #6*) during T_d, marked by the red dashed line in Fig. 7(d)−(f). A two-stage temperature growth is also observed during T_d in this case, with one from the compression effect of preceding shock and the other from the combustive heat release backwards. Whereas, there is a much smoother transition from the decoupling to coupling of the SF and RF for $X_{H_2} = 0.5$ in the accelerated recoupling period (i.e. line #8*-11* from 0.106 ms to 0.108 ms) than that for $X_{H_2} = 0.2$. Ahead of the RF marked by the black dashed line in Fig. 7(d)−(f), the new-formed forward-propagating SF relative to the lead shock occurs at around 0.106 ms (line #8*) with comparatively low intensity. The trailing complex of the original RF and new SF starts to gradually get close to the old SF until 0.108 ms (line #11*) when the two SF merge together. This process is accompanied by the increase of shock pressure from

Fig. 7 — Spatial profiles of (a) pressure, (b) temperature and (c) heat release rate with hydrogen volume fraction $X_{H_2} = 0.2$, the time stamps for lines 1−11 are: 1: 0.225 ms, 2: 0.227 ms, 3: 0.230 ms, 4: 0.235 ms, 5: 0.240 ms, 6: 0.245 ms, 7: 0.250 ms, 8: 0.255 ms, 9: 0.259 ms, 10: 0.260 ms, 11: 0.262 ms, and of (d) pressure, (e) temperature and (f) heat release rate with $X_{H_2} = 0.5$, the time stamps for lines 1*-11* are: 1*: 0.1 ms, 2*: 0.1005 ms, 3*: 0.101 ms, 4*: 0.102 ms, 5*: 0.103 ms, 6*: 0.104 ms, 7*: 0.105 ms, 8*: 0.106 ms, 9*: 0.107 ms, 10*: 0.1075 ms, 11*: 0.108 ms (equivalence ratio: 0.8, initial temperature: 300 K, initial pressure: 1 atm).

43.67 atm to 70.19 atm and HRR from 1.28×10^{13} J/m³/s to 8.07×10^{13} J/m³/s. Meanwhile, the temperature just behind the SF of the new detonative front gets back to about 2813 K at 0.108 ms for the next pulsation cycle.

As indicated in Fig. 4, stable detonation can be achieved with further increase in hydrogen volume fraction. Fig. 8 shows the spatial and temporal temperature and pressure gradient profiles in the detonated ammonia-hydrogen-air mixture with initial conditions (X_{H_2}, ϕ, p_0, p_{drive}, T_0 = 0.7, 0.8, 1 atm, 150 atm, 300 K). Stably propagating detonation is observed from 0.06 ms to 0.09 ms. It is found that the RF and SF are always coupled with a HRL of 1.01 mm and propagate forward synchronously. The steady detonation propagation is achieved for $f = 1.51$ and $r_p = 150$ in the mixture condition here, while the short-period pulsating detonation propagation has been observed by Yungster and Radhakrishnan [18] in hydrogen-air mixtures with initial conditions (ϕ, p_0, r_p, $T_0 = 0.8$, 0.42 bar, 140, 298 K or 0.8, 0.8 bar, 190, 298 K). This indicates that small amounts of ammonia addition to hydrogen (ammonia volume fraction in fuel $X_{NH_3} = 0.3$ here) can help obtain a stable detonation wave. Here, the shock pressure is around 36.9 atm, the HRR can reach 2×10^{13} J/m³/s, and the temperature of burned gas is over 3000 K, all of which are quite close to those of detonation propagation of a stoichiometric hydrogen-air mixture [57].

Effects of equivalence ratio

Previous studies have suggested pulsating instabilities of different fuel/air mixtures can behave differently with varying equivalence ratios [18,24]. Studies on the dynamics of ammonia/air mixtures autoignition have also highlighted significant differences between ammonia and hydrocarbon fuels, particularly methane [58]. Therefore, parametric studies were carried out over equivalence ratios varying from 0.6 to 2.5 for ammonia-hydrogen-air mixtures (initial conditions at: p_0, r_p, T_0, $X_{H_2} = 1$ atm, 150, 300 K, 0.2). Fig. 9 shows the variation of detonation speed with respect to time for different mixture compositions. Significant pulsating instabilities for the propagation of RF and SF are observed in all studied mixture compositions. The coupling (1−2), accelerated decoupling (2−3), and accelerated recoupling (3−4) relations of the two fronts are identified and marked in Fig. 9. It is found that both lean and rich mixtures pertain longer T_c and T_d periods compared to the stoichiometric mixture. This is consistent with the finding shown in the literature suggesting when activation temperature is low (near stoichiometric conditions) the duration of one pulsating detonation cycle decreases while the pulsating frequency increases [13,59]. The CJ speed, overdrive degree, oscillation frequency, and amplitude for all simulated cases are presented in Table 2. Note that although
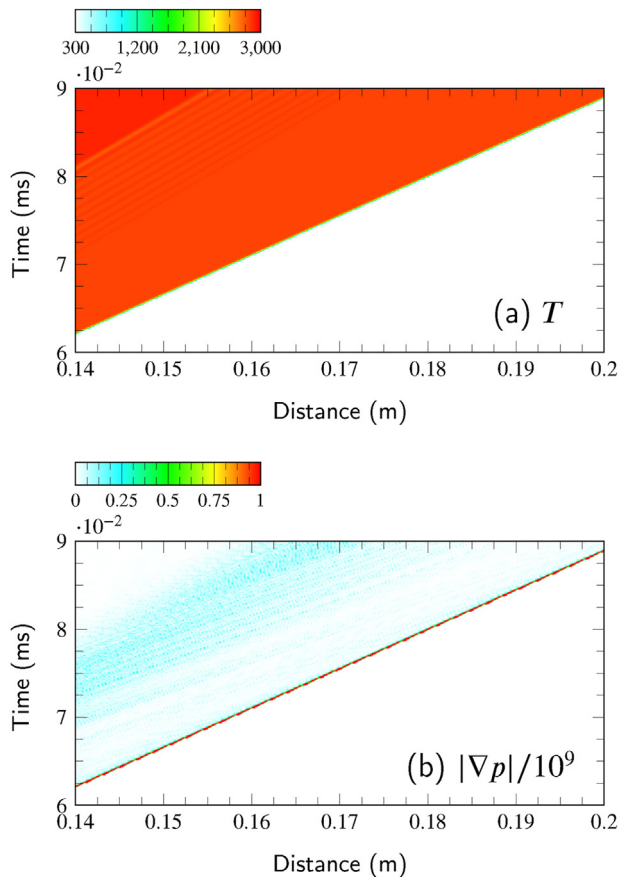
Fig. 8 — Spatial and temporal distributions of (a) temperature (in K), (b) pressure gradient (Pa/m) RF: reaction front; SF: shock front (hydrogen volume fraction: 0.7, equivalence ratio: 0.8, initial temperature: 300 K, initial pressure: 1 atm).

the driver pressure ratio is fixed for all cases, the degree of overdrive increases for both leaner and richer mixtures. Similar phenomena in hydrogen-air mixtures were reported by Yungster and Radhakrishnan [18]. The current study of ammonia/hydrogen blends suggests the CJ speed is peaked near stoichiometry, while the previous study on hydrogen-air mixtures suggested that the CJ speed increases monotonically when the equivalence ratio is between 0.4 and 2 [18]. Similar characteristics of ammonia/hydrogen blends that the laminar burning velocities (LBV) peak near stoichiometry in LBV measurements of ammonia/hydrogen mixtures have been reported [60]. The oscillatory amplitude $\Delta p/\bar{p}$ of the SF shows different trends compared to f, first rising from 0.83 for $\phi = 0.6$ to 0.92 for stoichiometry, then declining to 0.46 for $\phi = 2.5$ as the mixture getting richer.

The temporal and spatial distributions of temperature and pressure gradient for a fuel-lean ($\phi = 0.6$) and a fuel-rich ($\phi = 2.5$) ammonia-hydrogen-air mixture are shown in Fig. 10. Only one pulsation period is presented here for both lean (0.257–0.322 ms) and rich mixtures (0.185–0.246 ms). The transients observed in Fig. 5 are also observed here for both fuel-lean and fuel-rich conditions, including the coupling, accelerated decoupling, and recoupling periods of the RF and

SF, compression and expansion waves from shock bifurcations, and secondary reaction fronts (i.e. SRF). The temperature is elevated abruptly across the SRF due to chemical reactions of undetonated intermediate radicals, while it is found that the temperature behind the SRF is around 2700 K for $\phi = 0.6$, and 2500 K for $\phi = 2.5$, much lower than that of 3000 K for $\phi = 0.8$ in Fig. 5. The pressure gradient of SF in the fuel-rich premixture is lower than that of the fuel-lean counterpart for almost one order of magnitude as shown in Fig. 10(b) and (d).

The T_c of this pulsating cycle for $\phi = 0.6$ lasts between 0.257 ms and 0.262 ms. Thereafter, the first bifurcation B_1 separates the death and re-initiation of detonation at 0.303 ms when a new SF occurs ahead of the RF. Before the appearance of B_2, a trifurcation point marked as T_1 in Fig. 10(b) is observed at around 0.311 ms. A forward-propagating compressible wave is found to be accompanied by a series of relatively weak backward-propagating compression waves relative to the RF (marked as CW). The forward-propagating compressible wave appearing around T_1 finally merges with and strengthens the new-formed SF at around 0.317 ms. After this period, a new RF with increasing HRR is produced at around 0.319 ms and produces a new detonative front via the compression effects of the strengthened SF and the old lead SF at around 0.320 ms (B_2). This process can be further presented in Fig. 11 through spatial distributions of pressure and HRR over time between 0.314 ms and 0.320 ms. The RF is just behind the new-formed SF with the peak value of pressure at 0.314 ms. The two compression waves generated from T_1 are clearly marked in Fig. 11(a). The new-formed SF rapidly catches up and combines with the right-propagating compression wave relative to the RF at 0.317 ms, relatively far away from the RF, while close to the lead SF as Fig. 11(b) demonstrates. A new RF starts to appear due to the compression between the new and the original SF at around 0.319 ms; meanwhile, the CW_2 with a higher intensity than the left-propagating CW is produced. The growing HRR of the new-formed RF at 0.657 m has overtaken that of the old RF at 0.656 m from 0.320 ms, and turns the old RF to an intense reaction front (labelled in Fig. 11(d)). The trailing intense reaction front with evident heat release and pressure growth combines with the lead detonative front at B_3 of around 0.322 ms, accompanied with the occurrence of an expansion wave EW as Fig. 10(b) shows. During this accelerated recoupling period (0.303–0.322 ms), a detonation wave of coupled RF and SF is generated for the new pulsation cycle.

The physics and dynamics of one pulsating detonation cycle in the fuel-rich ammonia-hydrogen-air mixture ($\phi = 2.5$) is presented in Fig. 10(c) and (d). The duration of T_c is from 0.1855 ms to 0.189 ms, and then the accelerated decoupling of the RF and SF occurs until B_1 at 0.220 ms. Thereafter, it comes to the accelerated recoupling period (0.220–0.246 ms) of T_d. The generation of a new SF is observed closely ahead of the RF, and thus a developing detonative front is formed in the shocked gas behind the original SF, accompanied with a series of backward-propagating compression waves relative to the RF (i.e. CW). This new-formed detonative front propagates forward with a higher speed than and thus gradually approaches the SF. The second bifurcation B_2 occurs at 0.246 ms when the detonative front overtakes the SF and generates a
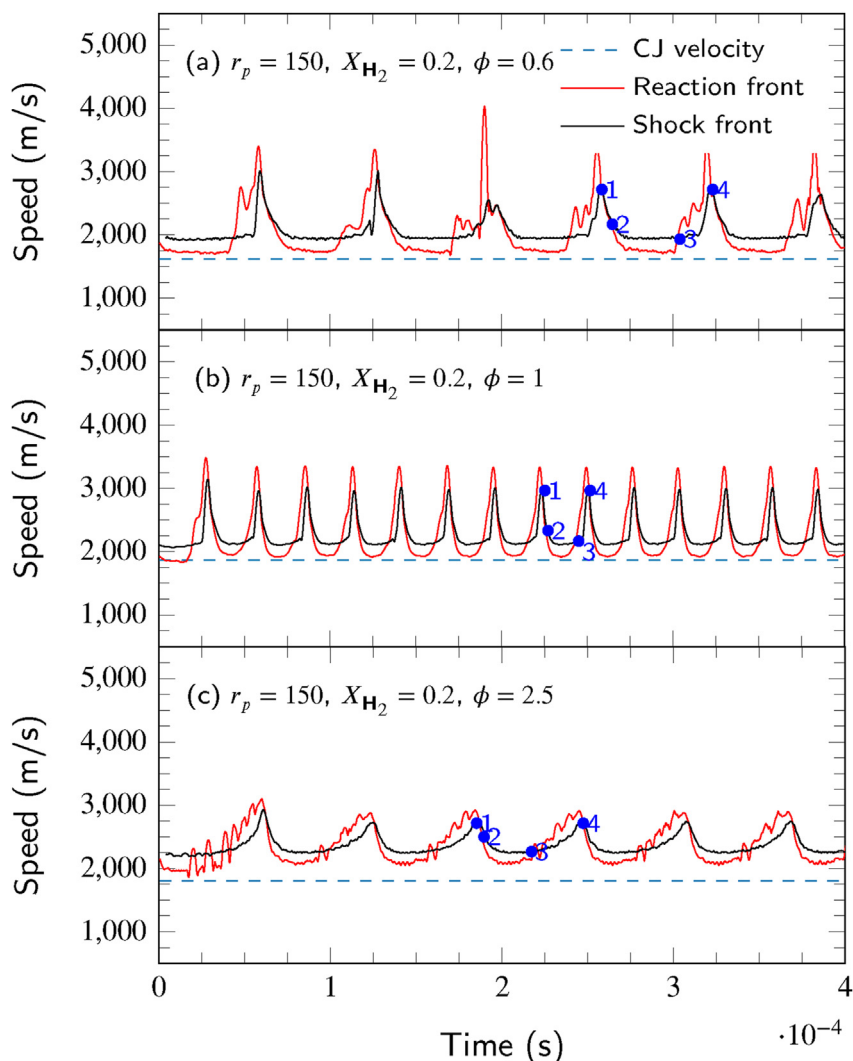
Fig. 9 — Time histories of propagation speeds of reaction and shock fronts with equivalence ratio of (a) $\phi = 0.6$, (b) $\phi = 0.7$ (c) $\phi = 1$, (d) $\phi = 2$, (e) $\phi = 2.5$ (initial temperature: 300 K, initial pressure: 1 atm, volume fraction of hydrogen in fuel: 0.2).

Table 2 — The CJ speed, overdrive degree, oscillation frequency and amplitude for various equivalence ratio ($p_0 = 1$ atm, $r_p = 150$, $T_0 = 300$ K, $X_{H_2} = 0.2$).

ϕ	D_{CJ} (m/s)	f	ω (Hz)	$\Delta p/p$
0.6	1619.04	1.62	15385	0.83
0.7	1698.34	1.57	21277	0.91
1.0	1870.29	1.49	35714	0.92
2.0	1853.03	1.63	23256	0.74
2.5	1804.97	1.74	16667	0.46

detonation wave for the next pulsation cycle; meanwhile, the formation of a backward-propagating expansion wave (i.e. EW) relative to the lead SF is found. Periodic interactions between the SF and RF of this pulsating detonation with only two bifurcation points are similar to those of fuel-lean n-heptane pulsating detonation propagation. However, a relatively complex process was observed in fuel-rich n-heptane-air premixtures suggesting different autoignition dynamics of ammonia/hydrogen blends [24].

Fig. 12 shows the spatial profiles of pressure and HRR in accelerated recoupling durations for both $\phi = 0.6$ and $\phi = 2.5$, corresponding to the same initial conditions and pulsating detonation cycles in Fig. 10. For $\phi = 0.6$, significant pressure rise is observed ahead of the RF from 0.309 ms to 0.317 ms as the forward-propagating compression wave occurring at around 0.311 ms (T_1) strengthens and merges into the new-formed SF, accompanied with the gradually increasing HRR. The original RF pressure abruptly rises from 43.59 atm at 0.317 ms to 57.17 atm at 0.320 ms due to the formation of a new SF with increasingly intense HRR in the shocked gas. The SF and RF are mutually enhanced in the process, leading to extremely high peak values of pressure (79.96 atm) and HRR (2.84×10^{13} J/m³/s). The eventual combination of the lead detonative front and following intense reaction front occurs at around 0.321 ms. The shock pressure and HRR of the new detonation front are 65.32 atm and 1.62×10^{13} J/m³/s, respectively. The transition from the decoupling to coupling of the SF and RF for $\phi = 2.5$ is much smoother than that for $\phi = 0.6$. The new SF generated in the shocked gas ahead of the RF almost has the same intensity with, and gradually
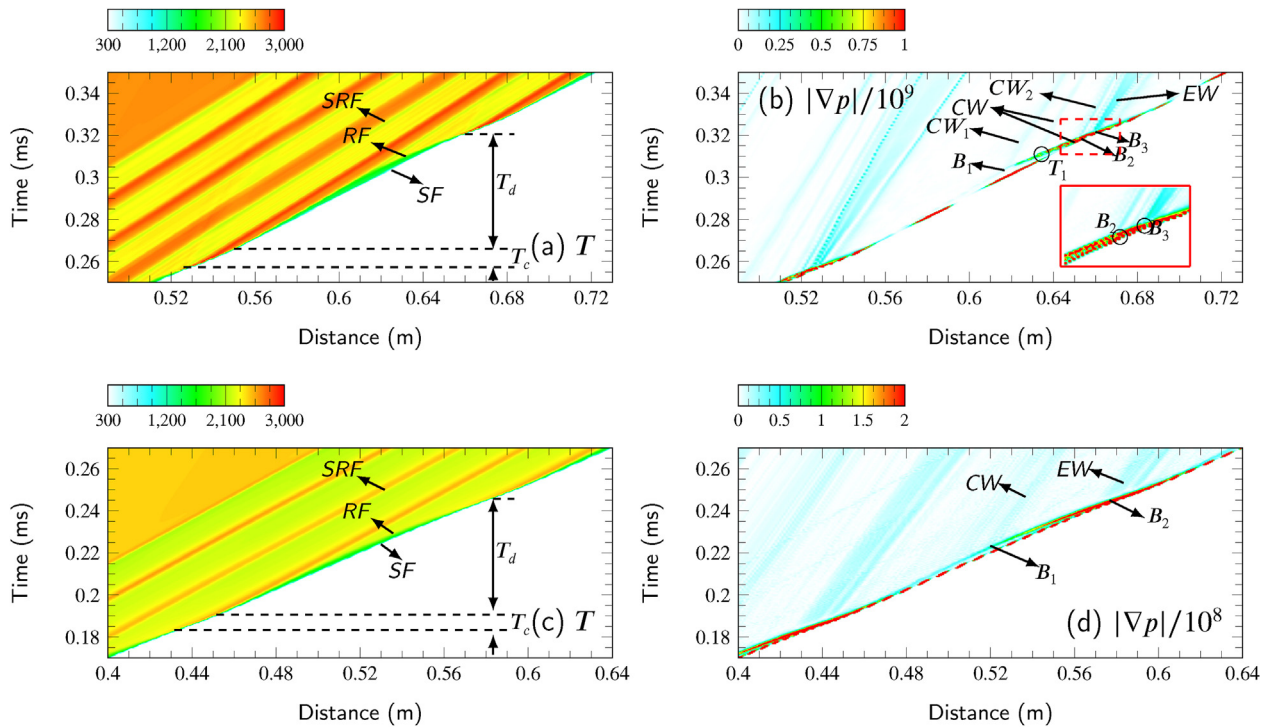
Fig. 10 — Spatial and temporal distributions of (a) temperature (in K) and (b) pressure gradient (Pa/m) with equivalence ratio $\phi = 0.6$, and of (c) temperature (in K) and (d) pressure gradient (Pa/s) with equivalence ratio $\phi = 2.5$. RF: reaction front; SRF: secondary reaction front; SF: shock front; CW: compression waves; EW: expansion wave; T_D: decoupling period; T_C: coupling period; B_1, B_2: bifurcation point (hydrogen volume fraction: 0.2, initial temperature: 300 K, initial pressure: 1 atm).

approaches the old SF from 0.235 ms to 0.246 ms. Meanwhile, the shock pressure rises from 48.23 atm to 61.40 atm, simultaneously the HRR increases from 1.67×10^{12} J/m^3/s to 5.95×10^{12} J/m^3/s. Then the coupled RF and SF start the next cycle of pulsating detonation. Both the shock pressure and HRR of detonation propagation for $\phi = 2.5$ are much smaller than those for lean conditions of $\phi = 0.6$ and 0.8 in ammonia-hydrogen-air mixtures, as indicated in Fig. 7(a)–(c) and Fig. 12.

The spatial distributions of ammonia (NH$_3$), hydrogen (H$_2$), medium molecule pyrolytic products from ammonia (NH$_2$), and nitrogen monoxide (NO) mass fractions from the same pulsating detonation cycle as in Fig. 10 are demonstrated in Fig. 13. Under the fuel-lean condition, premixed fuel of ammonia and hydrogen blends are almost completely consumed between the leading SF and trailing RF in the whole pulsating detonative combustion (line #1–11) as shown in Fig. 13(a) and (b). However, a considerable residual mass fraction of ammonia is found under the fuel-rich condition, and hydrogen is even produced from redundant ammonia decomposition, especially during coupling period with comparatively high temperature (about 2800 K) in the narrow induction zone, demonstrated in Fig. 13(e) and (f).

As for intermediate active radicals and oxidation products simultaneously, peaks of NH$_2$ first decrease in accelerated decoupling period (line #4–7 or line #4*-7*), and then increase in accelerated recoupling period (line #8–11 or line #8*-11*) with respect to time in Fig. 13(c) and (g), keeping pace with HRR peaks under both $\phi = 0.6$ and $\phi = 2.5$ conditions. This is consistent with the autoignition behaviour of ammonia/air

combustion where NH2 increases from the very start of the autoignition process as a result of the initial fuel decomposition [58]. The high temperature (over 3000 K) and corresponding HRR between the RF and SF when they are coupled in fuel-lean burned gas in Fig. 10(a) and Fig. 12(b) comes from the oxidation of medium or small pyrolytic products by ammonia, as evidenced by the rapidly reduced NH$_2$ and increased NO as Fig. 13(d) shows near the RF between 0.257 ms (line #1) and 0.262 ms (line #3). Large amounts of NO are generated from NH$_2$ oxidation within the coupling period, but much less when the RF and SF are decoupled from 0.309 ms to 0.320 ms (line #4–11). As the predominant pollutant in the fuel-lean detonated ammonia-hydrogen-air mixture, the residual mass fraction of NO is approximately 0.025 for $\phi = 0.6$. Whereas, differently, the production of NO is always synchronised with the HRR for $\phi = 2.5$ in Fig. 13(h), which first apparently produced due to the SF compression effects and then rapidly declines around the RF during both the coupling period from 0.186 ms (line #1*) to 0.191 ms (#3*) and the decoupling period from 0.196 ms (line #4*) to 0.230 ms (#11*). Meanwhile, the peak concentrations of NO are relatively high within T_c, but low within T_d, consistent with temporal variations of HRR. The peak values of NO mass fraction (0.004–0.009) are much lower than those in the fuel-lean case, and the concentration is around 0.0005 in the detonated gas, even below the detection limit. The spatial evolutions of NO between the SF and RF suggest that its formation and consumption process under fuel-rich conditions may have different dominant reaction paths from fuel-lean conditions.
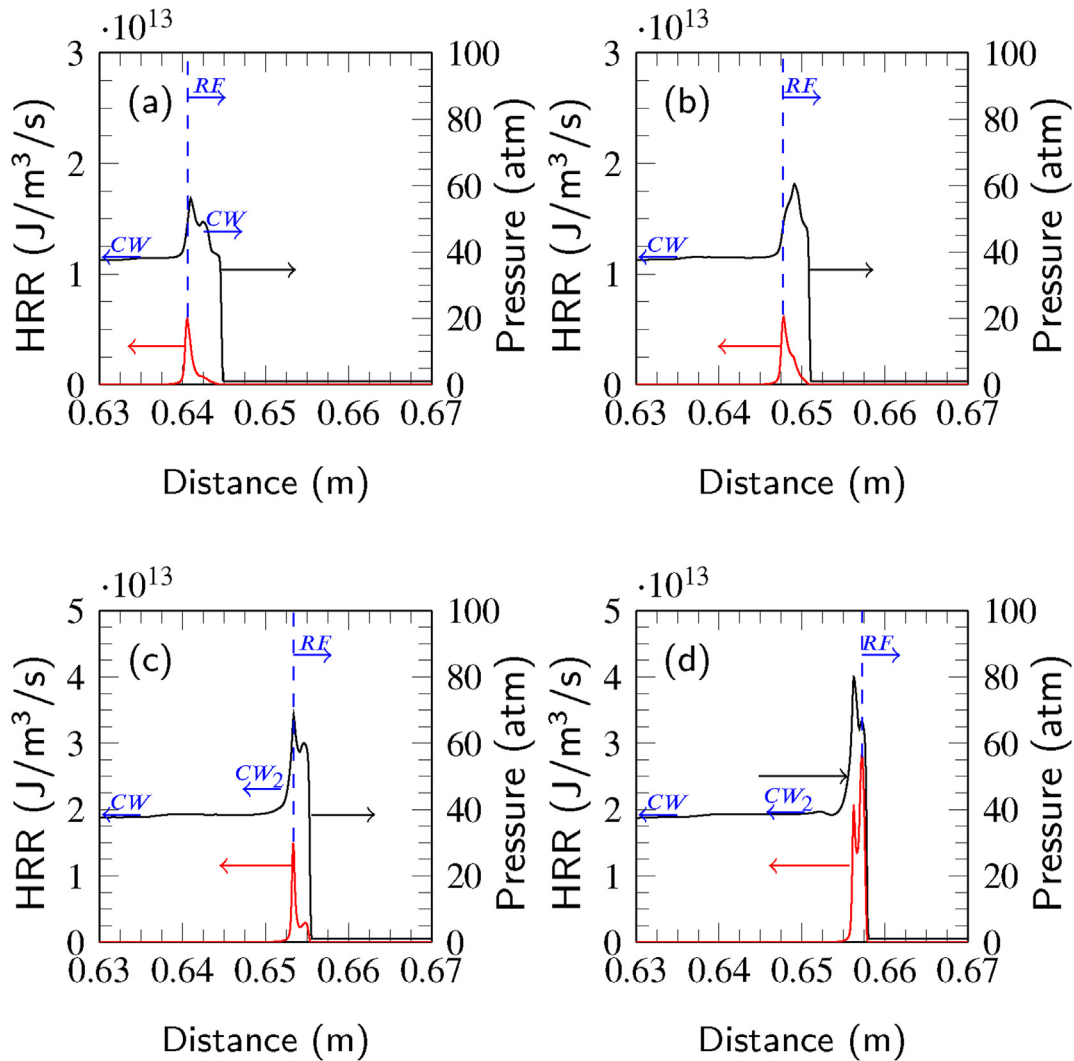
Fig. 11 — Spatial profiles of pressure and heat release rate at t = (a) 0.314 ms, (b) 0.317 ms (c) 0.319 ms and (d) 0.320 ms (hydrogen volume fraction: 0.2, equivalence ratio: 0.6, initial temperature: 300 K, initial pressure: 1 atm).

Chemical explosive mode analysis (CEMA)

In this study, the propagation mode of the combustion wave is investigated through a computational flame diagnostic tool, chemical explosive mode analysis (CEMA), first developed by Lu et al. [61]. CEMA characterises the propensity of a mixture to ignite in an isolated system, by analysing the chemical Jacobian of the local reactive system, described as

$$\frac{D\omega(\mathbf{y})}{Dt} = J_\omega \frac{D\mathbf{y}}{Dt} = J_\omega(\boldsymbol{\omega} + \mathbf{s}), J_\omega = \frac{\partial \boldsymbol{\omega}}{\partial \mathbf{y}} \tag{9}$$

where **y** is the vector of dependent variables (e.g. temperature and species mass fractions). $\boldsymbol{\omega}$ and **s**, respectively, are the chemical source term and the non-chemical source term associated with system. A CEM is identified when the chemical Jacobian (J_ω) has an unstable (i.e., explosive) eigenvalue characterised by a positive real part, λ_e, with the corresponding left eigenvector being b_e.

To further quantify interactions between chemistry and other processes, Xu et al. [62] projected Eq. (9) to the direction of CEM, resulting in:

$$\boldsymbol{b}_e \cdot \frac{D\omega(\mathbf{y})}{Dt} = \boldsymbol{b}_e \cdot J_\omega(\boldsymbol{\omega} + \mathbf{s}) = \lambda_e \boldsymbol{b}_e \cdot (\boldsymbol{\omega} + \mathbf{s}) \tag{10}$$

$$\frac{D\phi_\omega}{Dt} = \lambda_e \phi_\omega + \lambda_e \phi_s + \frac{D\boldsymbol{b}_e}{Dt} \cdot \omega \tag{11}$$

where

$$\phi_\omega = \boldsymbol{b}_e \cdot \omega, \quad \phi_s = \boldsymbol{b}_e \cdot \mathbf{s} \tag{12}$$

Xu et al. [62] further defined a local combustion mode indicator, α:

$$\alpha = \phi_s / \phi_\omega. \tag{13}$$

The value of α highlights the relative importance of the chemical source and non-chemical source terms, such as
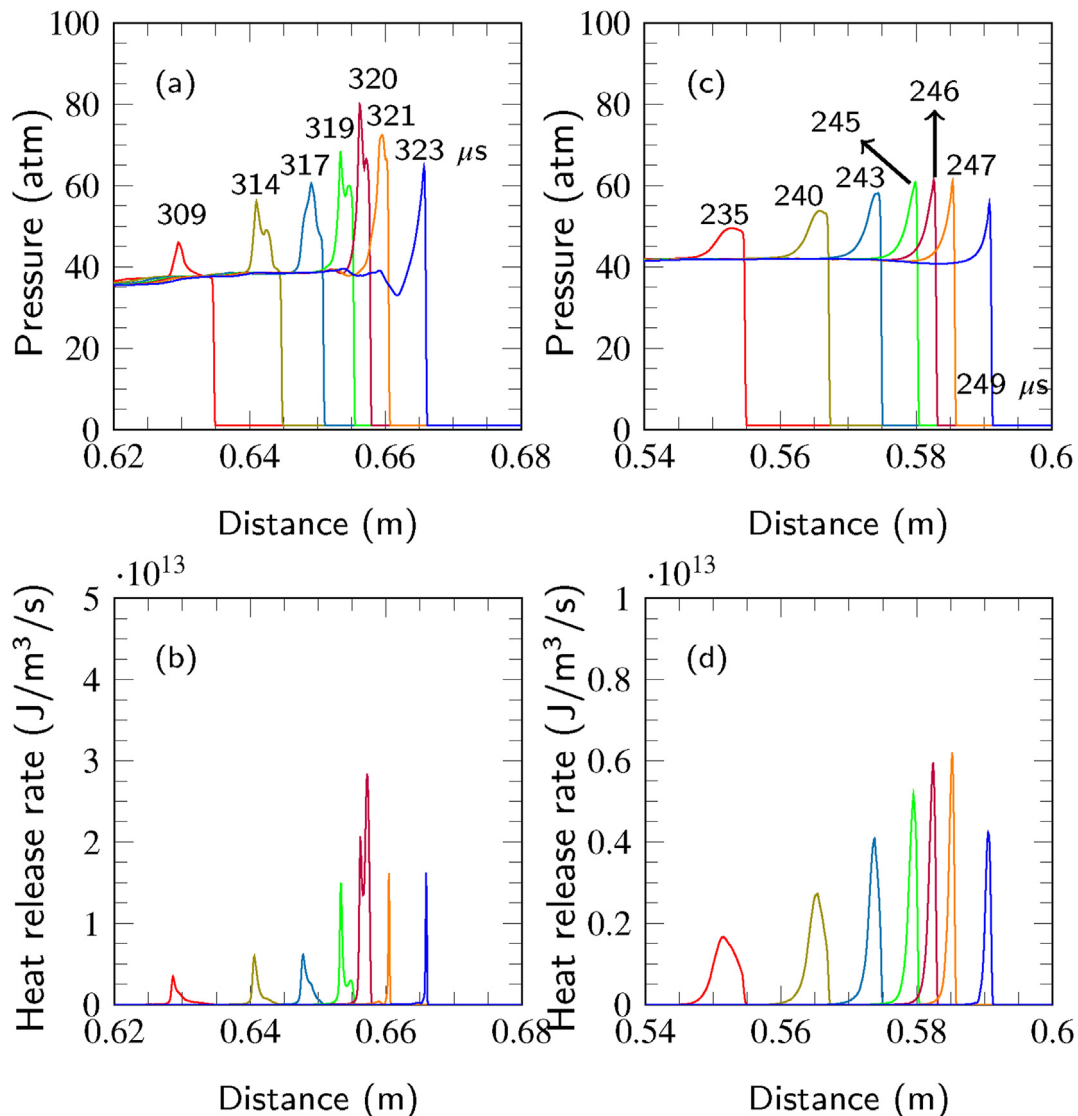
Fig. 12 — Spatial profiles of (a) pressure, (b) heat release rate with equivalence ratio $\phi = 0.6$, and of (c) pressure, (d) heat release rate with $\phi = 2.5$ (hydrogen volume fraction: 0.2, initial temperature: 300 K, initial pressure: 1 atm).

diffusion, in the ignition process. $\alpha \gg 1$ suggests diffusion dominates chemistry in promoting ignition, e.g., in the pre-heat zone of deflagrative flames, while detonation regime characterised by autoignition can be identified as $|\alpha| \ll 1$ where chemistry plays a dominant role. $\alpha \ll -1$ indicates the local extinction mode where diffusion dominates chemistry but reverses the ignition process. For a pulsating detonation cycle, it is worth studying the mixture combustion modes in both the coupling and decoupling periods.

As discussed before, mixture composition plays an important role in pulsating detonation. Therefore, CEMA analysis will focus on both lean and rich ammonia/hydrogen blends. Figs. 14 and 15 present the profiles of ϕ_ω and ϕ_s at various instants within the pulsating detonation cycles for $\phi = 0.6$ and $\phi = 2.5$. The spatial distributions of temperature are coloured by the CEM eigenvalue of $\mathrm{Re}(\lambda_e)$, whose positive value indicates the presence of explosive modes. The local combustion mode indicator, α, is shown in different colours

projected on the bottom horizontal line. The t_3, t_3^* are critical instants (i.e. instant 3 marked in Fig. 9), instants t_1-t_2, t_1^*-t_2^* are within the accelerated decoupling periods, whereas instants t_4-t_5, t_4^*-t_5^* are within the accelerated recoupling periods. It is found that both fuel-lean and fuel-rich ammonia-hydrogen-air mixtures are under chemically-frozen preignition conditions ahead of detonation waves (indicated by a near-zero eigenvalue). The gases in induction zones between the SF and RF become chemically explosive (indicated by large positive eigenvalues) due to shock compression and heating effects in both accelerated decoupling and recoupling stages, accompanied by temperature increases. The mixtures downstream of the RF are in non-explosive post-ignition states (i.e. marked as large negative eigenvalues and "Burn" by the combustion mode), indicating the mixtures are burned and evolving toward chemical equilibrium.

It is seen that the projected chemical source term ϕ_ω is significantly larger than the projected diffusion source term
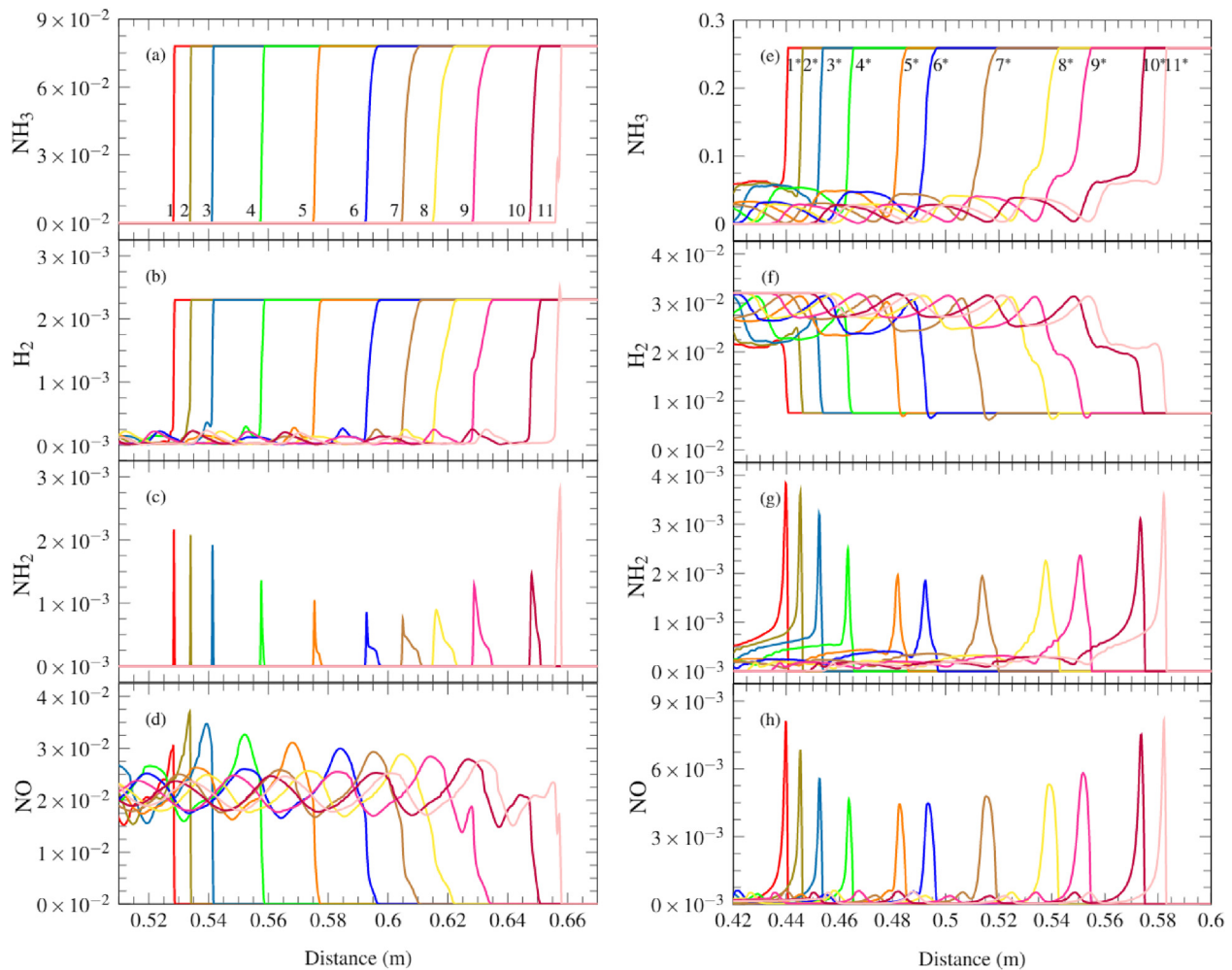
Fig. 13 – Spatial profiles of (a) NH_3, (b) H_2, (c) NH_2 and (d) NO with equivalence ratio of 0.6, the time stamps for lines 1–11 are: 1: 0.257 ms, 2: 0.259 ms, 3: 0.262 ms, 4: 0.270 ms, 5: 0.280 ms, 6: 0.290 ms, 7: 0.297 ms, 8: 0.303 ms, 9: 0.309 ms, 10: 0.317 ms, 11: 0.320 ms, and of (e) NH_3, (f) H_2, (g) NH_2 and (h) NO with equivalence ratio of 2.5, the time stamps for lines 1*-11* are: 1*: 0.186 ms, 2*: 0.188 ms, 3*: 0.191 ms, 4*: 0.196 ms, 5*: 0.205 ms, 6*: 0.210 ms, 7*: 0.220 ms, 8*: 0.230 ms, 9*: 0.235 ms, 10*: 0.243 ms, 11*: 0.246 ms (hydrogen volume fraction: 0.2, initial temperature: 300 K, initial pressure: 1 atm).

ϕ_s for the entire domain in all presented instants. This suggests that chemistry plays a more important role than thermal diffusion ($|\alpha| \ll 1$) in the decoupling and recoupling processes of the SF and RF under both lean and rich conditions, and thus the detonative front is propagating as a purely autoigniting front (marked by "Ign"). The current study is significantly different compared to the previous study by Zhao et al. [24] for n-heptane/air mixtures where during the decoupling-recoupling process non-negligible competition between thermal diffusion and chemical heat release may separate the induction zone into two parts: a preheat zone dominated by thermal diffusion immediately behind the shock front followed by an autoignition dominated reaction zone. Studies on other carbon-containing fuels also indicated that the autoignitive system can reside in the thermal runaway regime close to the end of the autoignition process. The current study also relates to the study by Wu et al. [63] which focused on premixed supersonic reactive hydrogen-air flows with and without shock waves. In that study, chemical contributions were seen to exceed non-chemical contributions in the mixture behind the lead shock wave in Chapman–Jouguet detonation and also behind the relatively high-speed deflagrative flame. In addition, the relative importance of chemical and diffusion process strongly depends on the temperature immediately after the shock. Xu et al. [62] have suggested that at a relatively high initial temperature, chemistry always plays a dominant role in a burner-stabilised hydrogen/air premixed flame configuration. Recent studies on ammonia autoignition behaviour have also suggested that, compared to other fuels, the ammonia system enters the thermal runaway regime relatively early during the autoigniton process and the steep increase in chemical runaway signifies the transition from the one regime to the other [58]. Their study also demonstrated that the portion of the ignition delay spanned by chemical runaway increases with initial temperature which in the current case is much higher than normal combustion. Therefore, the high driver pressure and high propagation
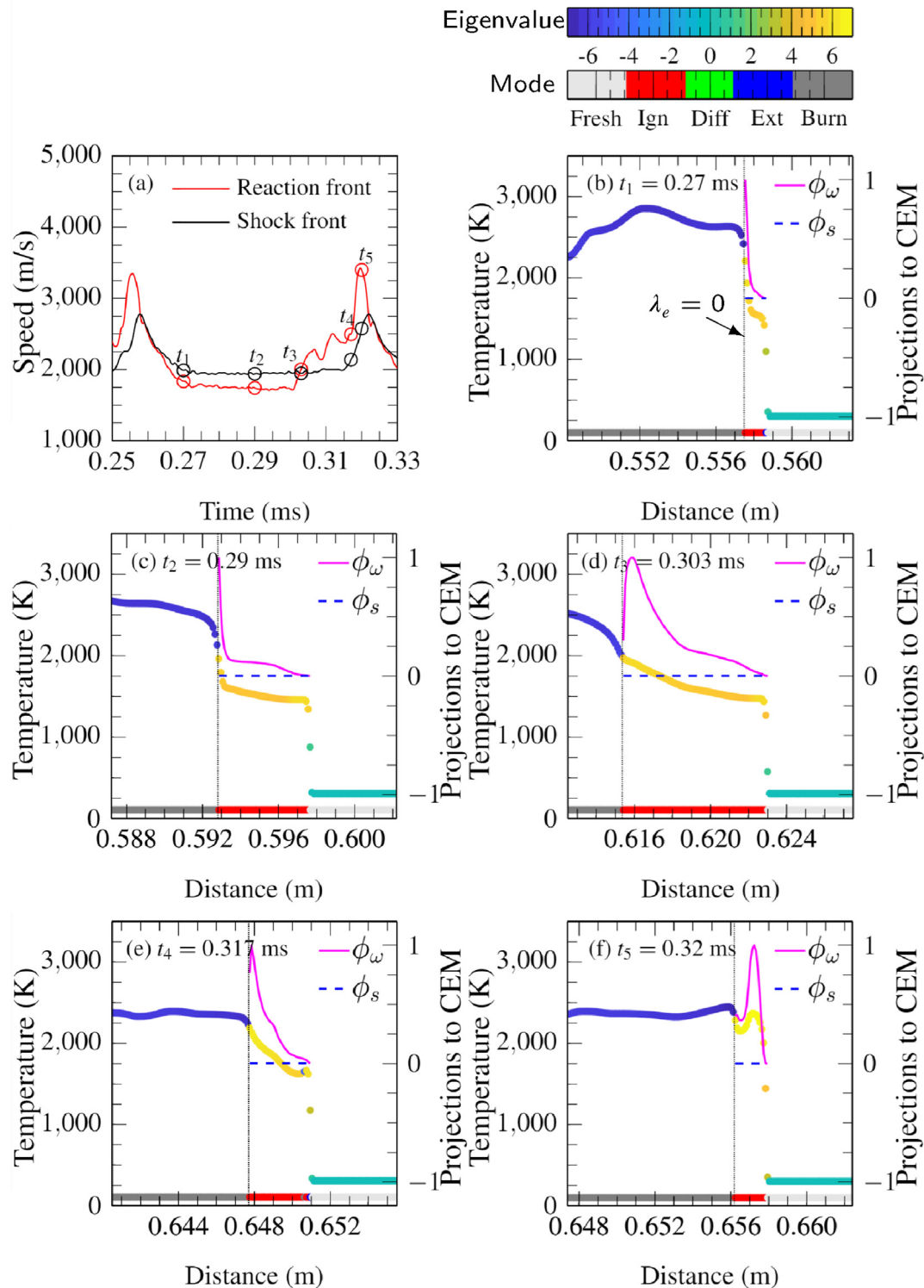
Fig. 14 — (a) Time evolutions of reaction and shock front propagation speeds and (b–f) distributions of temperature and normalised projections to CEM. Colours on temperature profiles are values of sign $(\lambda_e) \times \log_{10}(1 + ||\lambda_e||)$; while colours on the horizontal line indicate the auto-ignition mode (red, 'Ign', $|\alpha| \ll 1$), the diffusion assisted-ignition mode (green, 'Diff', $\alpha \gg 1$), the extinction mode (blue, 'Ext', $\alpha \ll -1$), non-explosive burned mixtures (grey, 'Burn', $\lambda_e < 0$), and fresh mixtures (light grey, 'Fresh', $T < 600K$). (hydrogen volume fraction: 0.2, equivalence ratio: 0.6, initial temperature: 300 K, initial pressure: 1 atm). (For interpretation of the references to colour in this figure legend, the reader is referred to the Web version of this article.)
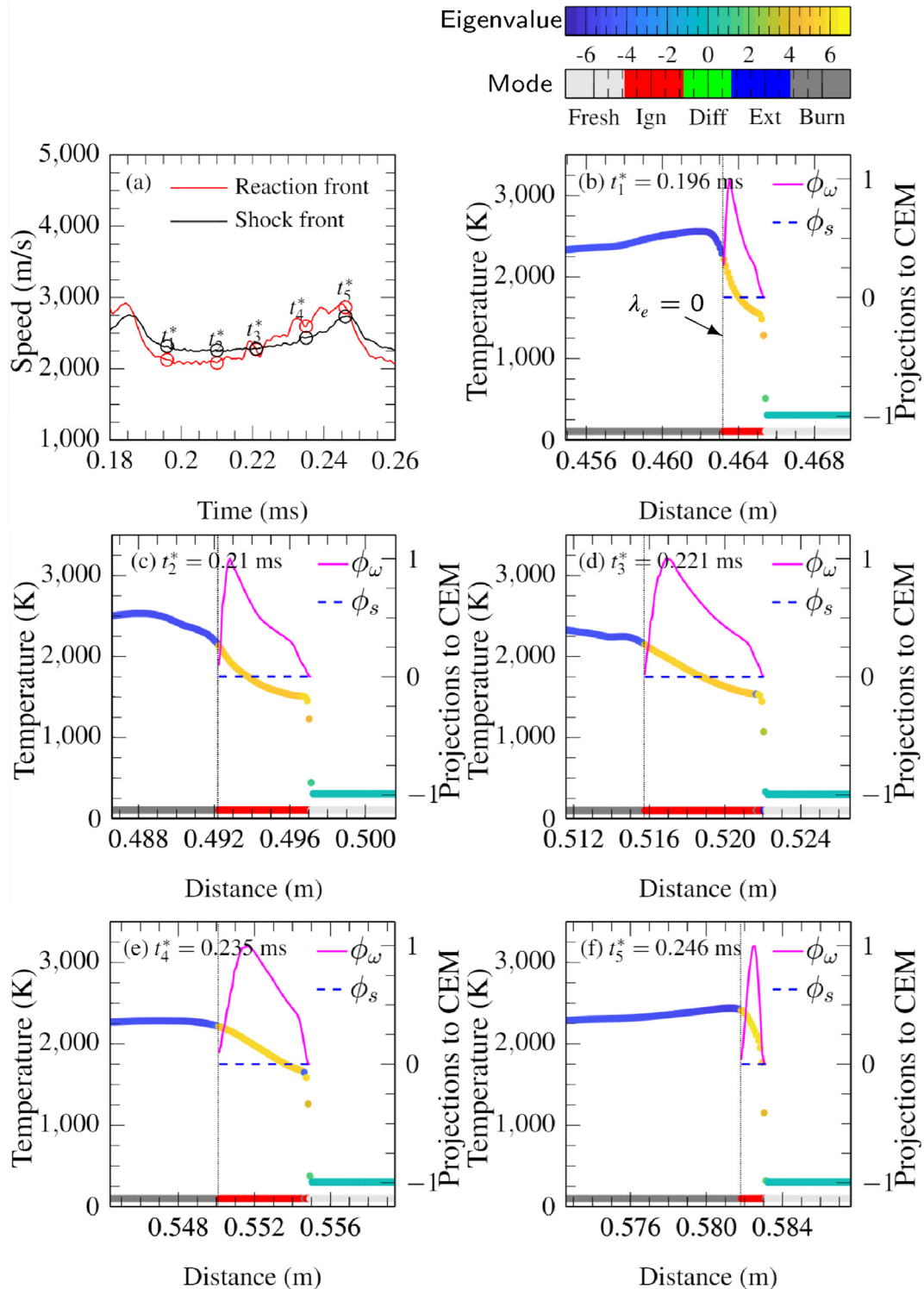
Fig. 15 – (a) Temporal evolution of reaction and shock front propagation speeds and (b–f) distributions of temperature and normalised projections to CEM. Colours on temperature profiles are values of sign $(\lambda_e) \times \log_{10}(1 + ||\lambda_e||)$; while colours on the horizontal line indicate the auto-ignition mode (red, $|\alpha| \ll 1$), the diffusion assisted-ignition mode (green, $\alpha \gg 1$), the extinction mode (blue, $\alpha \ll -1$), and non-explosive mixtures (grey, $\lambda_e < 0$). (hydrogen volume fraction: 0.2, equivalence ratio: 2.5, initial temperature: 300 K, initial pressure: 1 atm). (For interpretation of the references to colour in this figure legend, the reader is referred to the Web version of this article.)

speed induced high local temperature immediately after the shock front can lead to autoignitive dominated ammonia-hydrogen-air mixtures downstream of the SF seen in this study where the contribution of chemistry is prominent to the CEM rather than that of thermal diffusion.

Conclusions

Reactive Navier-Stokes equations coupled with the calorically perfect gas equation are numerically solved with a detailed chemical mechanism to investigate the propagation dynamics of pulsating detonations in a one-dimensional detonation tube filled with ammonia/hydrogen-air mixtures. A hot spot with high driver pressure and temperature is adopted to directly initiate the detonation wave. It is found, for the first time, that detonation can be initiated and propagate in ammonia/hydrogen-air mixtures, indicating their feasibility to be applied to detonation-based engines. The effects of hydrogen volume fraction in fuel, and fuel/air equivalence ratio on pulsating detonations are detailed. While the addition of hydrogen to ammonia suggests that stable detonation can be achieved at favourable conditions (i.e. high driver pressure), detonation and emission characteristics are found to be considerably affected by the blending fuel composition and equivalence ratio.

For a certain premixture, relatively low ratios between driver pressure to initial pressure exhibit highly unsteady oscillatory detonation propagation modes with low overdrive degrees. Under a constant pressure drive ratio of 150, the oscillation mode of pulsating detonation is considerably affected by hydrogen dilution in fuel blends. Evident pulsating instabilities with single frequencies are observed when the volume fraction of hydrogen in fuel is equal to 0.2, 0.3, and 0.5, and the transition from decoupling to coupling of shock front and reaction front becomes smoother with the addition of hydrogen in fuel. The phenomenon of "explosions in explosion" leads to the formation of a new detonation wave for the next pulsation cycle at the end of decoupling period, whereas a stable detonation with fixed travelling speed is achieved with a comparatively high hydrogen concentration in fuel of 0.7. When hydrogen accounts for 0.2 in fuel, pulsating detonation propagation with the regular decoupling and recoupling between lead shock wave and trailing reaction front occurs over an equivalence ratio from 0.6 to 2.5. Both fuel-lean and fuel-rich mixtures present lower oscillatory frequency compared to the stoichiometric mixture. The interactions between flame and shock fronts from decoupling to coupling relations are more complex under lean conditions than rich conditions. Nitrogen monoxide is the predominant pollutant in detonated mixtures for an equivalence ratio of 0.6, making up for approximately 0.025, but its residual mass fraction is only around 0.0005 for an equivalence ratio of 2.5. Considerable residual ammonia and hydrogen in the reacted fuel-rich gas may trigger explosions again if fresh air remixes with it. Further studies might be required to determine whether fuel-rich or fuel-lean ammonia/hydrogen-air mixtures are more appropriate for practical applications considering both thermal efficiency and emission requirements.

The chemical explosive mode analysis suggests that the mixture in the induction zone between reaction and shock fronts is highly explosive. Moreover, the contribution of chemical reactions always dominates that of thermal diffusion in the whole decoupling and recoupling periods under both lean and rich conditions, indicating that the propagating detonation pertains to a combustion mode of autoignition.

Declaration of competing interest

The authors declare that they have no known competing financial interests or personal relationships that could have appeared to influence the work reported in this paper.

Acknowledgements

Appendix A. Supplementary data

Supplementary data to this article can be found online at https://doi.org/10.1016/j.ijhydene.2022.04.265.

REFERENCES

[1] Roy G, Frolov S, Borisov A, Netzer D. Pulse detonation propulsion: challenges, current status, and future perspective. Prog Energy Combust Sci 2004;30(6):545—672. https://doi.org/10.1016/j.pecs.2004.05.001.

[2] Manabu H, Toshi F, Piotr W. Fundamentals of rotating detonations. Shock Waves 2009;19(1):1—10. https://doi.org/10.1007/s00193-008-0178-2.

[3] Williams FA. Combustion theory. CRC Press; 2018.

[4] Lee JHS. The detonation phenomenon. Cambridge University Press; 2008. https://doi.org/10.1017/CBO9780511754708.

[5] McVEY JB, Toong TY. Mechanism of instabilities of exothermic hypersonic blunt-body flows. Combust Sci Technol 1971;3(2):63—76. https://doi.org/10.1080/00102207108952273.

[6] Toong ARTY. Periodicity in exothermic hypersonic flows about blunt projectiles. NO 4-5 Astronaut. Acta; G.B.; DA. 1972;17:539—60. ABS. FR. RUSSE; BIBL. 18 REF.

[7] Han W, Gao Y, Wang C, Law CK. Coupled pulsating and cellular structure in the propagation of globally planar detonations in free space. Phys Fluids 2015;27(10):106101. https://doi.org/10.1063/1.4933134.

[8] Erpenbeck JJ. Stability of steady-state equilibrium detonations. Phys Fluid 1962;5(5):604—14.

[9] Daimon Y, Matsuo A. Detailed features of one-dimensional detonations. Phys Fluids 2003;15(1):112—22. https://doi.org/10.1063/1.1526698.

[10] McVey J, Toong T. Mechanism of instabilities of exothermic hypersonic blunt-body flows. Combust Sci Technol 1971;3(2):63–76.

[11] Alpert L, Ty T. Periodicity in exothermic hypersonic flows about blunt projectiles. 1972.

[12] Bourlioux A, Majda AJ, Roytburd V. Theoretical and numerical structure for unstable one-dimensional detonations. SIAM J Appl Math 1991;51(2):303–43. https://doi.org/10.1137/0151016.

[13] He L, Lee JHS. The dynamical limit of one-dimensional detonations. Phys Fluids 1995;7(5):1151–8. https://doi.org/10.1063/1.868556.

[14] Sánchez AL, Carretero M, Clavin P, Williams FA. One-dimensional overdriven detonations with branched-chain kinetics. Phys Fluids 2001;13(3):776–92. https://doi.org/10.1063/1.1345880.

[15] Ng HD, Radulescu MI, Higgins AJ, Nikiforakis N, Lee JHS. Numerical investigation of the instability for one-dimensional chapman–jouguet detonations with chain-branching kinetics. Combust Theor Model 2005;9(3):385–401. https://doi.org/10.1080/13647830500307758.

[16] Leung C, Radulescu MI, Sharpe GJ. Characteristics analysis of the one-dimensional pulsating dynamics of chain-branching detonations. Phys Fluids 2010;22(12):126101. https://doi.org/10.1063/1.3520188.

[17] Sussman M. A computational study of unsteady shock-induced combustion of hydrogen-air mixtures. In: 30th Joint propulsion conference and exhibit; 1994. p. 3101.

[18] Yungster S, Radhakrishnan K. Pulsating one-dimensional detonations in hydrogen–air mixtures. Combust Theor Model 2004;8(4):745–70. https://doi.org/10.1088/1364-7830/8/4/005.

[19] Han W, Wang C, Law CK. Pulsation in one-dimensional h2-o2 detonation with detailed reaction mechanism. Combust Flame 2019;200:242–61. https://doi.org/10.1016/j.combustflame.2018.11.024.

[20] Romick C, Aslam T, Powers JM. Verified and validated calculation of unsteady dynamics of viscous hydrogen-air detonations. J Fluid Mech 2015;769:154–81.

[21] Daimon Y, Matsuo A. Unsteady features on one-dimensional hydrogen-air detonations. Phys Fluids 2007;19(11):116101. https://doi.org/10.1063/1.2801478.

[22] Ma W, Wang C, Han W. Effect of concentration inhomogeneity on the pulsating instability of hydrogen–oxygen detonations. Shock Waves 2020;30:703–11. https://doi.org/10.1007/s00193-020-00976-7.

[23] Radulescu MI, Ng HD, Lee JH, Varatharajan B. The effect of argon dilution on the stability of acetylene/oxygen detonations. Proc Combust Inst 2002;29(2):2825–31. https://doi.org/10.1016/S1540-7489(02)80345-5.

[24] Zhao M, Ren Z, Zhang H. Pulsating detonative combustion in n-heptane/air mixtures under off-stoichiometric conditions. Combust Flame 2021;226:285–301. https://doi.org/10.1016/j.combustflame.2020.12.012.

[25] Gao Y, Zhang B, Ng HD, Lee JH. An experimental investigation of detonation limits in hydrogen–oxygen–argon mixtures. Int J Hydrog Energy 2016;41(14):6076–83. https://doi.org/10.1016/j.ijhydene.2016.02.130.

[26] Patel V, Shah R. Effect of hydrogen enrichment on combustion characteristics of methane swirling and non-swirling inverse diffusion flame. Int J Hydrog Energy 2019;44(52):28316–29. https://doi.org/10.1016/j.ijhydene.2019.09.076.

[27] Mardani A, Karimi Motaalegh Mahalegi H. Hydrogen enrichment of methane and syngas for mild combustion. Int J Hydrog Energy 2019;44(18):9423–37. https://doi.org/10.1016/j.ijhydene.2019.02.072.

[28] Tang C, Huang Z, Jin C, He J, Wang J, Wang X, Miao H. Laminar burning velocities and combustion characteristics of propane–hydrogen–air premixed flames. Int J Hydrog Energy 2008;33(18):4906–14. https://doi.org/10.1016/j.ijhydene.2008.06.063.

[29] Gonca G, Sahin B, Hocaoglu MF. Influences of hydrogen and various gas fuel addition to different liquid fuels on the performance characteristics of a spark ignition engine. Int J Hydrog Energy 2022;47(24):12421–31. https://doi.org/10.1016/j.ijhydene.2021.09.029. international Conference on Energy, Environment and Storage of Energy, 15. International Combustion Symposium.

[30] Frigo S, Gentili R. Analysis of the behaviour of a 4-stroke si engine fuelled with ammonia and hydrogen. Int J Hydrog Energy 2013;38(3):1607–15. https://doi.org/10.1016/j.ijhydene.2012.10.114. 2011 Zing International Hydrogen and Fuel Cells Conference: from Nanomaterials to Demonstrators.

[31] Valera-Medina A, Pugh D, Marsh P, Bulat G, Bowen P. Preliminary study on lean premixed combustion of ammonia-hydrogen for swirling gas turbine combustors. Int J Hydrog Energy 2017;42(38):24495–503. https://doi.org/10.1016/j.ijhydene.2017.08.028.

[32] Zamfirescu C, Dincer I. Using ammonia as a sustainable fuel. J Power Sources 2008;185(1):459–65. https://doi.org/10.1016/j.jpowsour.2008.02.097.

[33] Yu Z, Zhang H. End-gas autoignition and knocking combustion of ammonia/hydrogen/air mixtures in a confined reactor. Int J Hydrog Energy 2022;47(13):8585–602. https://doi.org/10.1016/j.ijhydene.2021.12.181.

[34] Zhu R, Zhao M, Zhang H. Numerical simulation of flame acceleration and deflagration-to-detonation transition in ammonia-hydrogen–oxygen mixtures. Int J Hydrog Energy 2021;46(1):1273–87. https://doi.org/10.1016/j.ijhydene.2020.09.227.

[35] Li Y, Bi M, Li B, Zhou Y, Huang L, Gao W. Explosion hazard evaluation of renewable hydrogen/ammonia/air fuels. Energy 2018;159:252–63. https://doi.org/10.1016/j.energy.2018.06.174.

[36] Xiao H, Valera-Medina A, Bowen PJ. Modeling combustion of ammonia/hydrogen fuel blends under gas turbine conditions. Energy Fuel 2017;31(8):8631–42. https://doi.org/10.1021/acs.energyfuels.7b00709.

[37] Poling BE, Prausnitz JM, O'connell JP. Properties of gases and liquids. McGraw-Hill Education; 2001.

[38] Huang Z, Zhao M, Xu Y, Li G, Zhang H. Eulerian-Lagrangian modelling of detonative combustion in two-phase gas-droplet mixtures with openfoam: validations and verifications. Fuel 2021;286:119402. https://doi.org/10.1016/j.fuel.2020.119402.

[39] Greenshields CJ, Weller HG, Gasparini L, Reese JM. Implementation of semi-discrete, non-staggered central schemes in a colocated, polyhedral, finite volume framework, for high-speed viscous flows. Int J Numer Methods Fluid 2010;63(1):1–21. https://doi.org/10.1002/fld.2069.

[40] Kurganov A, Noelle S, Petrova G. Semidiscrete central-upwind schemes for hyperbolic conservation laws and Hamilton–Jacobi equations. SIAM J Sci Comput 2001;23(3):707–40. https://doi.org/10.1137/S1064827500373413.

[41] Wanner G, Hairer E. Solving ordinary differential equations II: stiff and differential algebraic problems, vol. 375. Springer Berlin Heidelberg; 1996.

[42] Zhang H, Zhao M, Huang Z. Large eddy simulation of turbulent supersonic hydrogen flames with openfoam. Fuel 2020;282:118812. https://doi.org/10.1016/j.fuel.2020.118812.

[43] Zhao M, Chen ZX, Zhang H, Swaminathan N. Large eddy simulation of a supersonic lifted hydrogen flame with

perfectly stirred reactor model. Combust Flame 2021;230:111441. https://doi.org/10.1016/j.combustflame.2021.111441.

[44] Huang Z, Zhang H. Numerical investigations of mixed supersonic and subsonic combustion modes in a model combustor. Int J Hydrog Energy 2020;45(1):1045–60. https://doi.org/10.1016/j.ijhydene.2019.10.193.

[45] Zhao M, Li J-M, Teo CJ, Khoo BC, Zhang H. Effects of variable total pressures on instability and extinction of rotating detonation combustion, Flow. Turbul Combus 2020;104(1):261–90. https://doi.org/10.1007/s10494-019-00050-y.

[46] Zhao M, Cleary MJ, Zhang H. Combustion mode and wave multiplicity in rotating detonative combustion with separate reactant injection. Combust Flame 2021;225:291–304. https://doi.org/10.1016/j.combustflame.2020.11.001.

[47] Xu Y, Zhao M, Zhang H. Extinction of incident hydrogen/air detonation in fine water sprays. Phys Fluids 2021;33(11):116109. https://doi.org/10.1063/5.0071405.

[48] Xu Y, Zhang H. Pulsating propagation and extinction of hydrogen detonations in ultrafine water sprays. Combust Flame 2022;241:112086. https://doi.org/10.1016/j.combustflame.2022.112086.

[49] Song Y, Hashemi H, Christensen JM, Zou C, Marshall P, Glarborg P. Ammonia oxidation at high pressure and intermediate temperatures. Fuel 2016;181:358–65. https://doi.org/10.1016/j.fuel.2016.04.100.

[50] Manna MV, Sabia P, Ragucci R, de Joannon M. Ammonia oxidation regimes and transitional behaviors in a jet stirred flow reactor. Combust Flame 2021;228:388–400. https://doi.org/10.1016/j.combustflame.2021.02.014.

[51] Sabia P, Manna MV, Cavaliere A, Ragucci R, de Joannon M. Ammonia oxidation features in a jet stirred flow reactor. the role of nh2 chemistry. Fuel 2020;276:118054. https://doi.org/10.1016/j.fuel.2020.118054.

[52] Yungster S, Radhakrishnan K. Structure and stability of one-dimensional detonationsin ethylene-air mixtures. Shock Waves 2005;14(1):61–72.

[53] R. Mével, J. Melguizo-Gavilanes, N. Chaumeix, Detonation in ammonia-based mixtures, Asia-Pacific Conference on Combustion 11.

[54] J. E. Shepherd, The shock and detonation toolbox. URL http://shepherd.caltech.edu/EDL/PublicResources/sdt/.

[55] Wei H, Chen C, Shu G, Liang X, Zhou L. Pressure wave evolution during two hotspots autoignition within end-gas region under internal combustion engine-relevant conditions. Combust Flame 2018;189:142–54. https://doi.org/10.1016/j.combustflame.2017.10.036.

[56] Sharpe GJ, Falle SAEG. One-dimensional nonlinear stability of pathological detonations. J Fluid Mech 2000;414:339–66. https://doi.org/10.1017/S0022112000008697.

[57] Gamezo VN, Ogawa T, Oran ES. Numerical simulations of flame propagation and ddt in obstructed channels filled with hydrogen–air mixture. Proc Combust Inst 2007;31(2):2463–71. https://doi.org/10.1016/j.proci.2006.07.220.

[58] Manias DM, Patsatzis DG, Kyritsis DC, Goussis DA. Nh3 vs. ch4 autoignition: a comparison of chemical dynamics. Combust Theor Model 2021:1–22. https://doi.org/10.1080/13647830.2021.1890835. 0 (0).

[59] Sharpe GJ, Falle SAEG. One-dimensional numerical simulations of idealized detonations. Proc R Soc Lon Series A 1983;455:1203–14. https://doi.org/10.1098/rspa.1999.0355. 1999.

[60] Valera-Medina A, Xiao H, Owen-Jones M, David W, Bowen P. Ammonia for power. Prog Energy Combust Sci 2018;69:63–102. https://doi.org/10.1016/j.pecs.2018.07.001.

[61] Lu TF, Yoo CS, Chen JH, Law CK. Three-dimensional direct numerical simulation of a turbulent lifted hydrogen jet flame in heated coflow: a chemical explosive mode analysis. J Fluid Mech 2010;652:45–64. https://doi.org/10.1017/S002211201000039X.

[62] Xu C, Park J-W, Yoo CS, Chen JH, Lu T. Identification of premixed flame propagation modes using chemical explosive mode analysis. Proc Combust Inst 2019;37(2):2407–15. https://doi.org/10.1016/j.proci.2018.07.069.

[63] Wu W, Piao Y, Xie Q, Ren Z. Flame diagnostics with a conservative representation of chemical explosive mode analysis. AIAA J 2019;57(4):1355–63. https://doi.org/10.2514/1.J057994.